Advances in Materials Research, Vol. 1, No. 4 (2012) 311-347
DOI: http://dx.doi.org/10.12989/amr.2012.1.4.311

Bactericidal and wound disinfection efficacy of nanostructured titania

Abdul-Majeed Azad*[1], Asem Aboelzahab[2] and Vijay Goel[2,3]

[1]*Chemical Engineering Department, The University of Toledo, USA*
[2]*Bioengineering Department, The University of Toledo, 5051 Nitschke Hall, 2801 W. Bancroft St., Toledo, OH 43606-3390, USA*
[3]*Department of Orthopedic Surgery, The University of Toledo, Toledo, Ohio 435606-3390, USA*

(Received August 8, 2012, Revised September 27, 2012, Accepted October 31, 2012)

Abstract. Infections are caused due to the infiltration of tissue or organ space by infectious bacterial agents, among which *Staphylococcus aureus* bacteria are clinically most relevant. While current treatment modalities are in general quite effective, several bacterial strains exhibit high resistance to them, leading to complications and additional surgeries, thereby increasing the patient morbidity rates. Titanium dioxide is a celebrated photoactive material and has been utilized extensively in antibacterial functions, making it a leading infection mitigating agent. In view of the property amelioration in materials via nanofication, free-standing titania nanofibers (pure and nominally doped) and nanocoatings (on Ti and Ti6Al4V implants) were fabricated and evaluated to assess their efficacy to mitigate the viability and growth of *S. aureus* upon brief (30 s) activation by a portable hand-held infrared laser. In order to gauge the effect of exposure and its correlation with the antibacterial activities, both isolated (only titania substrate) and simultaneous (substrate submerged in the bacterial suspension) activations were performed. The bactericidal efficacy of the IR-activated TiO_2 nanocoatings was also tested against *E. coli* biofilms. Toxicity study was conducted to assess any potential harm to the tissue cells in the presence of photoactivated materials. These investigations showed that the photoactivated titania nanofibers caused greater than 97% bacterial necrosis of *S. aureus*. In the case of titania-coated Ti-implant surrogates, the bactericidal efficacy exceeded 90% in the case of pre-activation and was 100% in the case of simultaneous-activation. In addition to their high bactericidal efficacy against *S. aureus*, the benignity of titania nanofibers and nanocoatings towards tissue cells during in-vivo exposure was also demonstrated, making them safe for use in implant devices.

Keywords: titanium dioxide; doped-titanium dioxide; titanium implant; nanofibers; nanotubes; *staphylococcus aureus*; photoactivation; infra red laser; infection mitigation; electron microscopy; confocal microscopy

1. Introduction

The Centers for Disease Control and Prevention (CDC) consistently report annually on the top ten causes of death in the United States (Minino *et al*. 2002). These reports identify the top leading terminal causes of death as: heart disease, malignant neoplasms, cerebro-vascular disease and unintentional injury among several others. Some of the leading factors for death in the US can be

*Corresponding author, Professor, E-mail: abdul-majeed.azad@utoledo.edu

avoided or mitigated with simple lifestyle changes, such as by switching to a healthier diet. Several of these causes are more uncontrollable, such as the proliferation of microbial agents in our bodies that cause infection and damage biologic tissues. For this reason, effective methods of mitigating the onset of infection due to bacteria are an important focus in the world of medical research. Although developments in this area have come a long way, the detrimental damage caused by bacterial infections still remains a serious source of human illness and mortality.

Surgical site infections (SSIs) are major cause of increased patient hospitalization, costs and physical pain, which subsequently reduce patient comfort and pace of recuperation due to further complications, and in many cases, could lead to death, either due to infection itself or other concomitant problems. Surgical site infections account for 14-16% of all nosocomial (hospital acquired) infections (Smith *et al*. 2000), while specifically within the surgical patient population, SSIs account for 38% of infections (National Nosocomial Infections Surveillance 1999). These statistics clearly relate to the necessity of novel methods of mitigating SSI occurrence, which would impact a large population of hospitalized patients, especially in the events of surgery. Although an infection can be obtained from any normal daily activities, known as community associated infection, it is much more relevant in clinical settings. The complication of invasive surgery adds to the detrimental effect, making infection a more probable occurrence.

Patients who develop SSIs often have a poor quality of life as the pain associated with SSI is often times excruciating. Furthermore, treatment for SSI can be lengthy with continual pain and discomfort until resolved. Symptoms of SSI include fever, pain or tenderness, redness and fluid drainage at the surgical site (Center for Disease Control and Prevention 2012). In many cases, late diagnosis and lack or failure of treatment may allow for the SSI to propagate to a point where conventional non-invasive treatments are exhausted with no avail.

In more complicated procedures, such as spinal surgery, the rate of infection has been found to increase to approximately 3-12% of patients, especially in the cases of traumatic injuries (Beiner *et al.* 2003, Sasso *et al.* 2008, Levi *et al.* 1997, Stall *et al.* 2009, Calderone *et al.* 1996, Glassman *et al.* 1996, Griffiths 1995). Massie *et al*. (1992) report an infection rate in spine fusion procedures exceeding 6% when instrumentation is used, with *S. aureus* being the most common infectious agent found in patients. These infection rates increase in patients without normal host defense against these agents (Thalgott *et al*. 1991). The vitality of recognizing these infections preemptively is very important, especially in the case of spine surgery (Theiss *et al*. 1996, Rechtine *et al*. 2001). This may warrant more drastic treatment methods such as debridement of the tissue or implant in order to remove as much of the infected area as possible. This measure would require additional surgical procedures, leading to more prolonged hospitalization and discomfort to the patient. SSI leads to death in many cases.

Olsen *et al*. (2003) found an SSI rate of 2.8% due to spinal surgery over a study period of 4 years. These were due to spinal laminectomy and/or fusion procedures where both organ space and incisional SSI was noticed. Risk factors for increased SSI occurrence were: (1) postoperative drainage at surgical site, (2) using a posterior surgical approach, (3) completion of procedures from tumor resection and (4) obesity.

Orthopedic procedure is an added variable, which in many cases increases the likelihood of infection. The implantation of a foreign object in the body causes several changes, both biomechanically and physiologically. Implantation procedures may spark body's immune response by rejecting the implant or not allowing for normal physiologic function of various tissues. In addition, the implant provides a surface for bacterial agents to lodge on, with no immune response

necessarily taking place. In many cases, these implants which are made of metals, alloys and/or ceramics, create a friendlier environment for infection onset.

This effect is well-documented with infections being reported in all types of prosthetic implant procedures. Occurrence of infection has been reported in 0.7%, 1% and 2% of shoulder, hip and knee replacement surgeries, respectively, with 15% of these surgeries due to extremity trauma (Bohsali *et al*. 2006, Meehan *et al*. 2003, Murray *et al*. 2011). Approximately half of the 2 million nosocomial infections per year in the United States have been attributed to the presence of implanted devices (Darouiche 2004). Moreover, they require additional antibiotic treatments over longer time periods in addition to an increased necessity for surgical procedures as compared to non-implant related infections (Whitehouse 2002, Darouiche 2001).

SSI is most commonly caused by the *Staphylococcus aureus* (*S. aureus)* bacteria. *S. aureus* is the most commonly isolated of these bacterial species in clinical settings, reaching close to 20% (Styers *et al*. 2006, Deresinski 2005, Chambers 2001). In many cases, *S. aureus* has the ability to conform to bodily immune responses and build resistance to the body's ability to remove it. When this occurs, the bacterial agent is able to multiply, form layers of adhesive biofilms, and propagate infection in the body.

Because of the presence of *S. aureus* in the buildup of in-vivo infections, this species is the most studied in the fabrication of antibacterial products, infection models and novel development of treatment methods. Among *S. aureus* bacteria, two main strains are present as related to their clinical presence: methicillin-resistant *Staphylococcus aureus* (MRSA) and methicillin-susceptible *Staphylococcus aureus* (MSSA). Methicillin, a penicillin-related antibiotic, had been a very effective treatment of *S. aureus* buildup for years, but certain *S. aureus* isolates build a strong resistance towards their necrosis effect (Sieradzki *et al*. 2010, Howden *et al*. 2004, Siberry *et al*. 2003, Jones *et al*. 2008, Cosgrove *et al*. 2005). For the purposes of this study, MSSA was used during experimental in-vitro trials, which was a notable advancement on previous reports by our group with *Escherichia coli* (*E. coli*) (Azad *et al*. 2010, Azad *et al*. 2011).

Due to its historic presence, *S. aureus* has developed resistance to frequently used antibiotic treatment against SSI. Therefore, SSI treatment with antibiotics is not effective in many cases, where the infection continues to persist. In many cases, this requires additional surgical procedures, hospitalization and incurs higher cost. Furthermore, while other procedures (such as the use of a pulsed lavage) for removing the bacterial buildup physically are in place, in the case of SSI, this method generally requires surgical intervention to reach the infected area and clean with the lavage. This suffers from the increased probability of additional infections, because lavage is more effective in case of wound infection, where superficial wounds can be cleaned without needing any invasive procedures.

S. aureus resistance in patients in the United States was shown to have increased by 50% over the period from the 1980s to the early 21st century by the National Nosocomial Infections Surveillance System (NNISS) (Salgado *et al*. 2005, NNISS 2001). This is in addition to *S. aureus* related mortality reported between 15% and 60% (Cluff *et al*. 1968, Julander 1985). Sands *et al*. (2003) found that 84% of SSI infections occurred post-discharge, which causes more lag time in discovering the infection. Despite the fact that 63% of these infections were successfully treated without the need for surgery, it still leaves close to 40% requiring invasive or other treatmens (Sands *et al*. 1996). It has been reported that approximately two thirds of infections in patients are caused by *S. aureus* and its sub-species (Darouiche 2004). Additionally, the persistence of infection in many cases is due to the capability of these agents to form biofilms, causing tight attachments of

cells to each other and to a surface.

The total cost of infection treatment in the United States alone was estimated to be over $4.5 billion in 1996, owing to the occurrence of various infections, including SSI (Jarvis 1996). Engemann *et al*. (2003) found the median hospital cost of patients with MRSA infection to be $92,363. It was less in the case of MSSA. Increased costs due to MRSA infection compared to MSSA infected or uninfected patients have also been reported by others (Cosgrove *et al*. 2005, Abramson *et al*. 1999, Chaix *et al*. 1999, Kim *et al*. 2001).

Aside from physical patient impact factors due to SSI, such as pain, discomfort and hospitalization, economic impact also highlights the importance of more comprehensive treatments for SSI. The healthcare costs associated with SSI occurrence are very significant, due to the physical factors a patient experiences. Perencevich *et al*. (2003) showed that the average post-discharge (8 weeks) cost for patients with SSI was $5,155, as compared to $1,773 for control patients with no infection. This amounts to an increase in cost by almost $3,400.

In a broader study of hospital associated infections (HAI), Klevens *et al*. (2007) estimated the occurrence of HAI in the US, and the number of resulting deaths. The study showed that in 2002, there were approximately 1.7 million cases of HAI as reported by hospitals and federal facilities, with the majority affecting patients outside of intensive care units (ICU). In relating subsequent deaths by type of infection, most deaths were a result of pneumonia, bloodstream and urinary tract infections, with each costing $35,967, $30,665 and $13,088, respectively. SSI-related death totaled 8,205. In 2002 alone, the total death toll due to HAI was almost 100,000, by correcting the association between antibiotic treatment resistance and subsequent outcomes such as mortality, morbidity. The cost increase was up to 100% with respect to treatable infections (Carmeli *et al*. 1999, Cosgrove *et al*. 2002, Holmberg *et al*. 1987).

Thus, in the light of the limitations of current treatments, a more innovative and less invasive path to mitigate SSI is needed. In this study, such a method is explored, using self-standing titanium dioxide (titania; TiO_2) nanofibers and nanocoatings on titanium and titanium alloys. Titania is photoactive, making it a viable candidate for creating a feasible treatment for SSIs. The premise of this work is therefore to study titania nanofibers on one hand, and nanocoatings on implantable materials on the other, for their efficacy towards disinfection and wound healing.

The significance of this lies in the fact that the treatment mechanism is novel to bacterial species as compared to antibiotics, thereby eliminating any resistance capability by the bacteria. This would reduce the limitation of antibiotic use in some cases where resistive bacteria are not found. Additionally, this is adaptable to both superficial wound infections as well as deep tissue infections in the case of orthopedic prostheses or implants. This also makes it viable to activate the implanted material at the time of surgery, with the possibility of subsequent activation either through surface penetration by the light source, or by the minimally invasive needle laser technology. Finally, this work is novel in the use of infrared source for activation of titania, compared to activation by ultraviolet light used previously by others.

1.1 Photocatalytic properties of titanium dioxide

The photocatalytic properties of titanium dioxide have been known since the early 1900's. The incorporation of titanium dioxide as white pigment in paint and fabric manufacturing allowed this capability to be first discovered due to the flaking of paint and fabric degradation. This was due to the instability of titania under ultraviolet (UV) light, since, it was discovered that exposure to

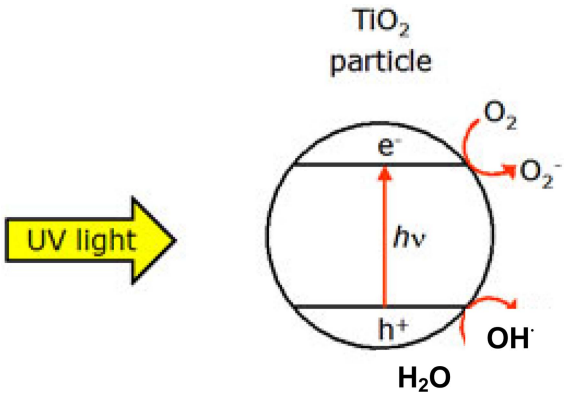

Fig. 1 Mechanism of TiO_2 photocatalysis

sunlight whose spectrum includes UV band, initiates a radio/photochemical reaction with titanium dioxide in these materials (Keidel 1929); this led to the possibility of using titania in photocatalysis. The photocatalytic properties of titanium dioxide were observed by Fujishima *et al*. (1969), in the photo-induced cleavage of water molecules, known as the Honda-Fujishima effect (Fujishima *et al*. 1972), on TiO_2 electrodes. Since then, photocatalysts based on titania have been extensively studied for the past 40 years, mainly for the destructions of organic compounds in water and in the environment. Titania is a semiconducting oxide with a bandgap of 3.2 eV. The general scheme of the photoactive process on titania surface triggered by UV radiations is shown in Fig. 1 (Destaillats 2012). Upon illumination by light, the photoenergy generates an electron-hole pair which comes to the surface, as shown below:

$$TiO_2 \xrightarrow{h\nu} e^-_{cb}(TiO_2) + h^+_{vb}\,(TiO_2) \tag{1}$$

The electron in the conduction band can reduce O_2 molecule and produce superoxide ions (O_2^-), and the hole in the valence band can react with H_2O and produce hydroxyl radical ($OH^\bullet$). Both these reactive oxygen species (ROS) are short-lived but extremely potent.

In addition, other ROS such as hydrogen peroxide and singlet oxygen radicals have also been detected. The reaction of ROS with organic compounds is extremely agile leading to their complete oxidation to carbon dioxide. The process of cell destruction in the case of living microorganisms also involves this oxidation mechanism, where the photo-induced generation of these reactive oxygen species (ROS) creates a hostile environment that mitigates bacterial proliferation and survival, thereby inducing bacterial cell necrosis (Cabiscol *et al*. 2000, Simon *et al*. 2000).

Killing of microbial cells in contact with a Pt-TiO_2 catalyst in water, upon illumination with near-UV light for 1 to 2 h was first reported by Matsunaga *et al.* (Matsunaga *et al*. 1985). It should be pointed out that in the absence of O_2 or other suitable electron acceptor, no photocatalytic reaction is likely to occur, due to the equally rapid and deleterious process of electron-hole recombination (Wei *et al*. 1994).

The effective activation of titania with UV light has been extensively reported, with ROS efficacy seen in most cases after 1 or 2 h of exposure (Koseki *et al*. 2009, Yu *et al*. 2003, Oka *et al*. 2008). However, the use of other activation sources has not been explored much and, is the main distinction of the present work from what has been reported in the published literature.

1.2 Antibacterial properties of titanium dioxide

Bacterial species proliferate and thrive in an environment with a normal oxidative state; a change in this scenario can be detrimental to their survival. The ability of TiO_2 to produce ROS upon photoactivation is linked to its inherent antibacterial behavior. As stated above, the ROS, though short-lived, are highly energetic and active, and thus can be detrimental to live microorganisms in their vicinity.

The photocatalytic/antibacterial behavior of titania nanoparticles and their ability to inhibit bacterial proliferation by inducing bacterial cell necrosis has been extensively reported. The efficacy of self-standing electrospun TiO_2 nanofibers and nanofilm coatings on Ti substrates (plates and wires), in initiating the necrosis of *E. coli* cells upon brief activation by infrared radiation has also been demonstrated recently (Azad *et al*. 2010, Azad *et al*. 2011). Others have investigated the propensity of ultraviolet (UV) activated TiO_2 powders and coatings (Koseki *et al*. 2009, Yu *et al*. 2003, Oka *et al*. 2008). However, in these cases, exposure for much longer duration (up to 2 h) was necessary to obtain significant bacterial death.

2. Techniques, materials and methods

The titania nanostructures were fabricated in two formats: (1) as free-standing nanofibers by electrospinning and (2) nanocatings on Ti and/or TiAl6V4 substrates. Due to the need of a novel method of SSI mitigation that could be used in conjunction with the current methods of treatment in vogue, the work reported here has obvious relevance. For example, titania in both these geometries can be easily integrated into current devices, such as prosthetics, wound patches, bandages, etc. The well-documented previous work with titania supports the proposed hypothesis, and the application to clinical situations where cases of currently untreatable SSI exist.

2.1 Electrospun nanofibers of titanium dioxide

Electrospinning (e-spinning) has been used as a technique for material fabrication for decades, including fabrics, tubular products, vascular grafts and others (Simons 1966, Bornat 1982, How 1985). More recently, e-spinning has been used as an advantageous method for producing biocompatible nanofibers of various materials that aid in the advancement of tissue engineering, such as extracellular matrix (ECM) construction, a method of cell-seeding and other applications (Zhang *et al*. 2005, Boland *et al*. 2006, Suwantong *et al*. 2010). This offers an important advantage to this fabrication technique in the growing arena of biocompatible materials, drug delivery and tissue engineering, and in solving biological problems. It allows for potential use in the inclusion of antibacterial properties in artificial blood vessels, tissue matrices and wound healing products (Zhang *et al*. 2005, Boland *et al*. 2006, Suwantong *et al*. 2010, Sill *et al*. 2008, Chen *et al*. 2005).

2.1.1 Preparation of polymeric and titanium precursors

The pure and doped titania fibers in non-woven format were fabricated by electrospinning using an indigenously assembled set-up, described in details elsewhere (Azad *et al*. 2010). Titanium (IV) oxynitrate [$TiO(NO_3)_2$] was used as the titanium precursor while water soluble iron (III) nitrate and silver (I) nitrate served as the source chemicals for iron and silver doping, respectively. For the

preparation of titanium oxynitrate (TON) solution, 0.6 g of titanium powder (-200 mesh, 99.5%, Alfa-Aesar) was dissolved in a mixture of 20 mL HNO_3 (ACS grade) and 30 mL H_2O_2 (ACS grade, 69.5% w/w). The solution was left under constant stirring overnight on a stir plate to form 0.4 M TON. The liquid was filtered into a clean container, discarding the remaining solid. This stock solution was stored at room temperature.

To prepare the 5 *wt*% Fe-doped TON solution, 100 mg of ferric nitrate ($Fe(NO_3)_3$, Alfa-Aesar, 98+ %) was dissolved in 100 mL of DI water. 50 μL of this solution was added to 5 mL of TON solution made earlier. The solution was thoroughly stirred magnetically to homogenize and stored at room temperature.

The Ag-doped TON solution was made following a similar protocol. A 0.1 M solution of silver nitrate was prepared by dissolving 168.7 mg of $AgNO_3$ (Alfa-Aesar, 99.9+ %) in 10 mL of DI water. 290 μL of this was added to 27 mL of TON, stirred thoroughly and stored at room temperature. This gives spinnable 1 *wt*% Ag-doped TON solution.

Polyvinyl pyrollidone (PVP) with an average molecular weight of 1.3×10^6 Dalton was dissolved slowly in ethanol to obtain its 15 *wt*% solution. The mixture was heated at approximately 60°C with constant stirring on a heat/stir plate. Once PVP fully dissolved forming a viscous solution, the solution was covered and capped tightly and stored at room temperature. Due to the pronounced volatility of ethanol during and after the preparation, and the tendency of the solution to dry out and leave a stiff gel in the container upon prolonged storage, the PVP solution was prepared in small batches and only when electrospinning was to be carried out.

2.1.2 Electrospinning TN/PVP solution and nanofiber formation

For electrospinning (e-spinning) experiments, the precursors were mixed in different ratios that were arrived at by several optimization trials. The liquid volume/volume (*v*/*v*) ratios of 1:2 for pure TON + PVP, 1:2 for silver nitrate-TON + PVP and 1:3 for iron nitrate-TON + PVP were found to yield the best results. Respective mixtures were made by mixing the inorganic and organic precursors and stirring magnetically for 2 min. into homogeneous viscous solutions.

Each of the three composite mixtures was drawn into an array of ten 5-mL capacity clinical syringes. Precision-tip 25 gauge stainless steel needles were attached to each syringe, and the entire array was mounted on a programmable syringe pump (KD Scientific model 230, MA). The preferred orientation of the syringe pump in this work was horizontal. A custom-made direct current power supply with a high voltage system (30 kV maximum) described earlier was used for e-spinning (Azad *et al*. 2008, Azad *et al*. 2010). One terminal of the power supply was connected to a metallic wire that looped through all the needles.

For the ease of sample handling and subsequent thermal processing, ceramic plates instead of metallic ones were used as the collector terminal. Moreover, in order to enhance the fiber collection area, a modified collection set-up was devised. Two high density alumina containers (76.2 mm long $\times$ 50.8 mm wide $\times$ 6.35 mm deep) were employed. The two containers were placed next to each other. Short lengths of electrical wires were attached to the back of each plate at their center by 1-sq. inch blocks of aluminum foil stuck by electrical tape. The other ends of the electrical leads were twisted into a common junction for the collector.

Using the high-voltage power supply, an electrical impulse was applied between the needle and the collectors in order to initiate the e-spinning. The syringe pump was started and the high-voltage supply unit was turned on. The voltage was tweaked precisely until the fibers began to form steadily and collect on the plates placed 63.5 mm away from the tip of the needle; the optimized

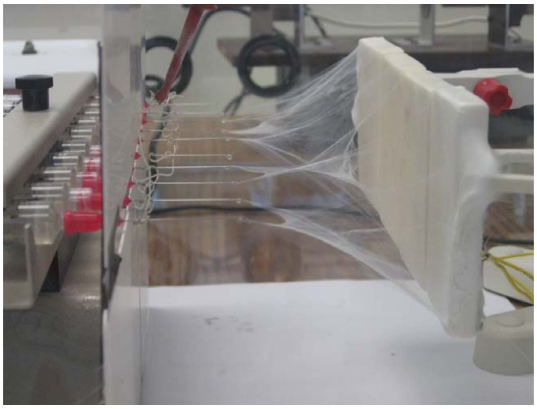

Fig. 2 Progress of electrospinning and collection of the non-woven ceramic-polymer (cermer) composite on the ceramic plates

voltage in this case was found to range between 16 and 18 kV. A flow rate of 0.05 ml/h was chosen and found to be adequate. The cermer (ceramic-polymer) composite fibers were spun continuously with short intermittent interruptions of the run for periodic cleaning of the clogged needle tips from time to time. Fig. 2 shows the experimental set-up for electrospinning and the non-woven matt of the electrospun cermer composite deposited on the collector plates with time.

2.1.3 Processing and characterization of the electrospun-fibers

After spinning was complete, small amounts of the as-spun composite fibers were used for viewing under scanning electron microscope. This allowed one to ensure the quality of fibers in terms of the absence of intertwining, twisting, branching, liquid globule entrapment, etc. The remaining fibers collected on the ceramic plates were fired at 700°C for 2 h in static air as per the following heating rate-temperature-soak time profile: 25°C (room temperature) to 500°C at a rate of ½°/min. with a hold at 500°C for 2 h; 500°C to 700°C at a rate of ½°/min. with a hold at 700°C for 2 h, followed by cooling from 700°C to the room temperature at a rate of ½°/min. The rather small heating and cooling rates were chosen so as to ensure the removal of organic components without destroying the nanofibrillar morphological features in the end product and also to avoid the disintegration of the nanofibers into a powdery mass. The final product was pure TiO_2 in one case and, TiO_2 doped with Ag and Fe_3O_4 in the other two.

The fired samples were characterized by a host of techniques, such as, powder X-ray diffractometry (XRD- PANalyticalX'Pert Pro MPD), scanning electron microscopy (Hitachi S-4800 UHR SEM) and transmission electron microscopy (Hitachi HD-2300 STEM), both with attachments capable of carrying out energy dispersive spectroscopy (EDS).

2.2 Coatings on implant surrogates

In addition to fabricating the self-standing electrospun titania nanofibers as described above, another practical and clinically relevant portion of this study was devoted to the creation of titania nanocoatings on titanium (Ti) and titanium alloy implant surrogates. Ti is a major component in various prosthetics and implantable devices, and is more commonly used in alloy form containing

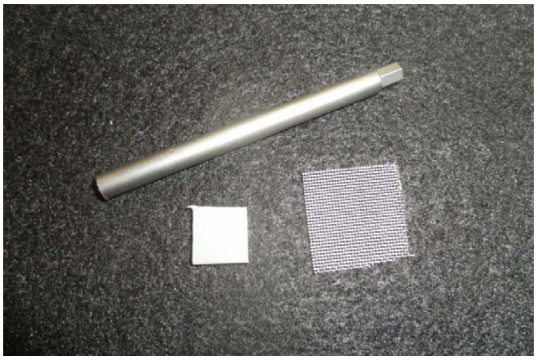

Fig. 3 As-received Ti plate, mesh and Ti6Al4V rod substrates

6 *wt*% aluminum and 4 *wt*% vanadium, commercially known as Ti6Al4V. Both these materials were used as substrates to assess their antibacterial efficacy and coating potency. TiO_2 coatings and/or films have been studied extensively, to explore methods of reducing the dependence on UV photoactivation and attempting to create doped formulations to attune for activation by visible light (Sarra-Bournet *et al*. 2011). In this work coatings were created by two processes, viz., aqueous plasma electrodeposition (PED) and anodization.

Titanium plates (of commercial purity 99.99%, Alfa-Aesar, MA) and titanium mesh (99% purity, Cleveland Wire Cloth & Manufacturing Company, OH) were used as implant surrogates. Additionally, clinically implantable Titanium-6Aluminum-4Vanadium (Ti6Al4V) extra low interstitial (ELI) spinal rod implants were also used in coating and bactericidal experiments. The use of diverse materials also permitted a direct comparison between the nanostructured morphologies formed on each, as well as their corresponding bactericidal potency. The as-received substrates are shown in Fig. 3.

2.2.1 TiO_2 coating on cp Ti plate, mesh and rod by plasma electrodeposition process

The three titanium implant surrogates were coated by Henkel Corporation (Madison Heights, MI, USA) using a patented aqueous plasma electrodeposition (PED) process. The method employs a pulsed DC voltage of 240 V for 10 ms on and 30 ms off with a current density of 1500 A/m^2, which creates a very adherent TiO_2 coating from the precursor solution on the substrate. In this case, each of the Ti substrates was used as the anode, onto which titanium dioxide deposits are created from solution; the coatings are cured *in situ* by the plasma glow on the surface (Azad *et al*. 2008, Azad *et al*. 2012). By increasing the time of PED process, sequentially thicker titania coatings were obtained on the Ti substrates. The TiO_2-coated samples were subsequently heated to 800°C for 4 h in static air at a ramp rate of 10°/min in both heating and cooling cycles.

Systematic structural and microstructural analysis of the samples was carried out using X-ray diffraction (XRD-PANalyticalX'Pert Pro MPD) and scanning electron microscopy (Hitachi S-4800 UHR SEM). The quantitative elemental analysis was accomplished by using the energy dispersive spectroscopy (EDS) attached to the SEM unit. Prior to SEM imaging, the sample surfaces were sputter-coated with a gold-palladium target for approximately 40 s. While the coated plates and rods were analyzed with both XRD and SEM/EDS, the analysis on mesh sample was done by SEM/EDS alone because of the difficulty of doing XRD on mesh configurations.

2.2.2 TiO_2 coating by anodization

Ti specimens were also coated by another technique which involved their anodization in acidic solution. This method has been successfully used previously to coat both mesh and plates with titania (Azad *et al*. 2011), but in the present case mesh surrogates were the focus. Anodization of Ti-alloy rods was also attempted, but was unsuccessful, due likely to the variation in their composition.

The TiO_2 coatings created by anodization possess quite different morphology than those from PED process; in the case of anodization, nanotubes formed on the Ti surface. For example, Mohapatra *et al*. (2007) produced titania nanotubes by anodizing a 0.2 mm thick Ti foil in an acidic mixture of 0.5 M phosphoric acid (H_3PO_4) and 0.14 M sodium fluoride (NaF) at 20 V assisted by sonication. In the present work, the solution consisted of a mixture of 0.5 M H_3PO_4 (Fisher Scientific, MA, USA) and 0.14 M hydrofluoric acid (HF, Alfa-Aesar, MA, USA) in DI water.

The solution was placed in a beaker inside a sonicator, with the mesh or plate immersed inside it; sonication aided in anodizing the entire surface uniformly. The Ti sample to be coated was connected to the positive terminal of the voltage source by a copper lead wire. Two lead wires attached to the negative terminal were individually connected to two platinum wires immersed on either side of the substrate. Use of two Pt wires ensured the anodization of both sides of the substrate. The duration of anodization was varied between 15 and 60 min., at an interval of 15 minutes; 30 min. period was found to be optimal. The anodized specimen were washed with DI water, dried and heated to 800°C for 4 h following a heating and cooling ramp rate of 10°C.

2.3 Bacterial growth

For bacterial growth, two sub-culture flasks with 150 mL of TSB superbroth (32 g of tryptone, 20 g of yeast extract and 5 g of sodium chloride per 1L DI water, Fisher Scientific, Waltham, MA) were inoculated with 1 mL of *S. aureus* (NRS72, Sanger476; MSSA), which was taken from a previously purified batch culture growth. A standard calibration curve was created with the aid of streaking of cell suspensions on TSB/agar to enumerate cell concentration. The *S. aureus* cells were grown to stationary phase, diluted to a concentration of 9.52×10^8 cells/ml, and then divided into 1 mL aliquots in 3 mL capacity eppendorf tubes for individual experiments. Stock solutions were also stored in 1 mL aliquots with the addition of 30% glycerol for future growth of more bacterial samples. All samples were stored at -80°C until use.

2.4 Infrared activation procedure

Ti mesh and plates followed a protocol of IR activation pre-placement amongst the bacterial suspension. Plate and mesh samples (1 cm × 1 cm) were placed on a sterile surface and activated by a handheld IR laser (λ = 808 nm; power = 1 W/cm^2, FreakLasers, China), shown in Fig. 4.

The laser activation time was kept constant at 30 s in all trials, holding the source approximately 2.5 inches away from the specimen. The activated sample was then placed using sterile forceps inside the microwell dish, among the bacterial suspension with the activated side facing down. Placement was done with extreme care in order to not invoke any mechanical stress on the bacterial suspension or cause any splashing of the liquid suspension.

Titania nanofibers were activated following a slightly different method, which involved placement of the fibers first in the bacterial suspension. This was followed by activating the samples by exposing the IR laser beam to the bottom side of the microwell dish, to ensure proper activation of

Fig. 4 Portable IR laser used for the photoactivation of titania

the fiber area contacting the suspension. This variation was due to the structural difference between fibers and plates/mesh and the difficulty in activating the fibers outside of the suspension.

Simultaneous activation procedure was applied to the Ti6Al4V rods and anodized Ti mesh. The reason for this was to compare the difference between pre-activation and simultaneous activation. In this procedure, samples were placed within the bacterial suspension in the microwell dish with the coated side facing down and activated as were the fibers.

2.5 In-situ confocal imaging and analysis

For analysis and imaging of cell necrosis of the bacterial suspension during experimentation, an Invitrogen Baclight Live/Dead Assay kit (Invitrogen, Carlsbad, CA) was used in addition to confocal microscopy to obtain real-time imaging of the bacterial cells while in suspension with the titania-coated Ti substrates, upon being activated by the IR laser. This assay uses SYTO9 and propidium iodide stains, which were stored in 1 μl aliquots for individual experimental use.

100 μL of *S. aureus* suspension were diluted in ultra-pure water (with a conductivity of 5.5×10^{-8} S-cm) to a 1:3 *v*/*v* ratio to a volume of 300 μL and cell concentration of 3.17×10^{8} cells/ml, with SYTO9 and PI stains added in 1 μL quantities, respectively. The suspension was set in the dark for 20 min. to complete staining. 10 μL of the suspension was then mixed with 30 μL of ultra-pure water (to cause 4-fold dilution) and added to a 35 mm × 14 mm glass bottom microwell dish (No. 15 cover glass). This gave a final concentration of 7.93×10^{7} cells/ml for imaging.

A 1 × 1 cm TiO_2-coated Ti specimen was first activated by the handheld IR laser (λ = 808 nm; power = 1 W) for 30 s, then introduced to the bacterial suspension. This laser introduces much greater power than the IR flashlight used in previous studies (Azad *et al*. 2008, 2010, 2011). The time-lapse imaging was recorded for 40 min. using a confocal multiphoton microscope system (Leica TCS SP5 MP, Leica Microsystems, Bannockburn, IL). Upon photoexcitation, the *S. aureus* cells stained with SYTO9 fluoresce green and those stained with propidium iodide fluoresce red. The excitation/emission of SYTO9 and propidium iodide occur at 480/500 nm and 490/645 nm, respectively. The survival/necrosis rate of the microorganism was determined by using the imaging software called ImageJ (image processing and analysis in Java – National Institute of Health; http://rsbweb.nih.gov/ij/download.html). By post-confocal imaging, this software allows one to count the bacteria in order to determine the number of live cells compared to total number of cells.

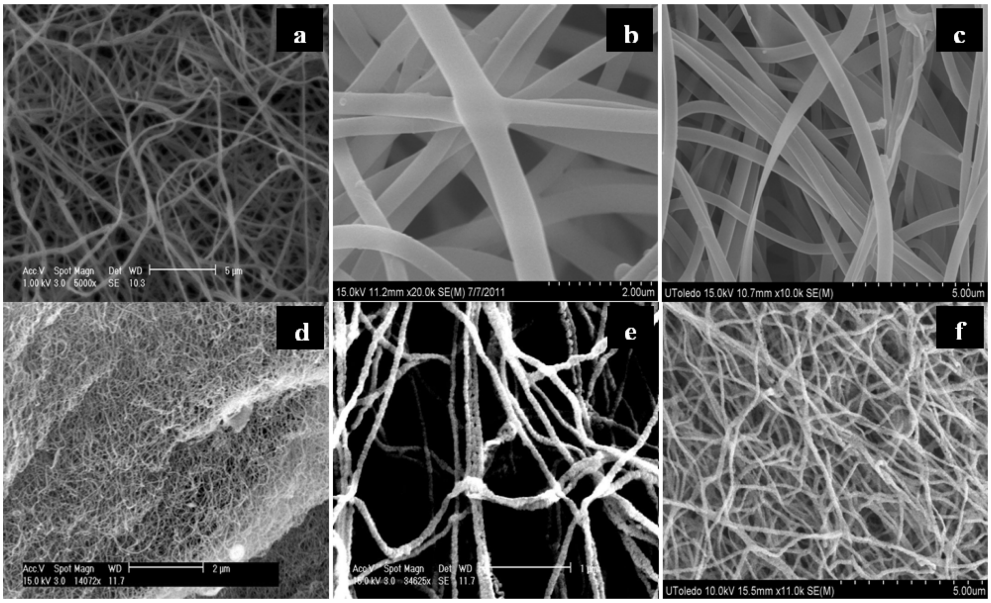

Fig. 5 SEM images of the as-spun (top) and calcined (bottom) fibers: (a,d) pure, (b,e) Fe-doped and (c,f) Ag-doped TiO_2

3. Results and discussion

3.1 Structural and elemental characteristics of titaniafibers and coatings

3.1.1 Electrospunnanofibers

The morphologies of the as-spun composite *cermer* (ceramic-polymer) fibers and the calcined (700°C/2 h) ceramic fibers both revealed presence of individual fiber strands. Due to the presence of polymeric component, the fiber diameter was larger in the as-spun sample. Approximate measurement using the high magnification SEM images shown in Fig. 5 indicated the diameter of the as-spun fibers of pure as well as Fe- and Ag-doped TiO_2 to be between 500 and 800 nm.

In comparison, the average diameter of the calcined fibers was approximately 150 nm. Previous analysis of these fiber specimens under transmission electron microscopy (TEM) showed the composition of the calcined fibers to consist of nearly monosized grains, approximately 20-25 nm in diameter, which were interconnected to form the continuous fiber (Azad *et al*. 2010). Calcination leads to the elimination of carbonaceous material, assigning porous attributes to the structure; this creates an added benefit for biocompatibility, wherein the porosity allows for quicker integration of the materials with surrounding physiological structures (Shi *et al*. 2002).

Moreover, small particle size is believed to enhance the effect of photoactivity. It has been shown that with particle size reduction, TiO_2 becomes more efficient at absorbing radiation as compared to large particles. The study attributes this phenomenon to the larger surface area per unit mass in the case of nanosized particles (Mao *et al*. 2006). This characteristic is vital in applications which rely on the ability to activate the materials with a light source. Similar observations have been made with other semiconducting oxides, such as zinc oxide (ZnO), which demonstrated increased

Table 1 EDS analysis of the as-spun and calcined pure TiO_2 fibers

Sample	As-spun TiO_2 Nanofibers		Calcined TiO_2 Nanofibers	
Element	Weight percent	Atomic percent	Weight percent	Atomic percent
Oxygen (O)	48.19	73.58	42.73	65.98
Titanium (Ti)	51.81	26.42	57.27	34.02

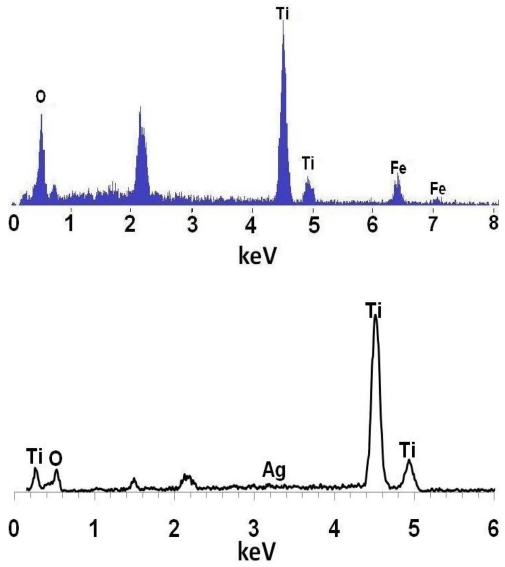

Fig. 6 EDS spectra of the Fe-doped (top) and Ag-doped (bottom) TiO_2 nanofibers, after calcination at 700ºC/2 h

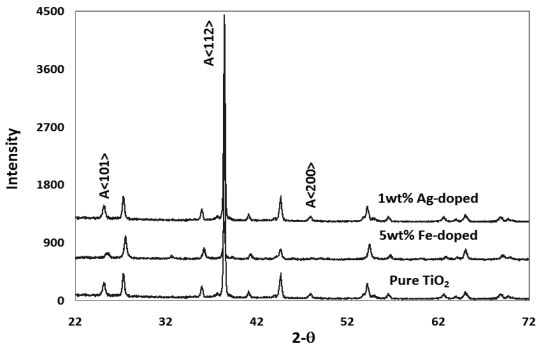

Fig. 7 XRD patterns of pure, Fe-doped and Ag-doped titania nanofibers

antibacterial activity due to reduced particle size (Emami-Karvani *et al*. 2011).

The EDS and XRD analyses on the as-spun and calcined fibers are shown in Table 1 and Figs. 6 and 7.

The XRD signature of the calcined samples conformed to that of TiO_2 in anatase and rutile phase; once formed, rutile is well-known for its excellent thermodynamic stability. Phase transitions in

titania has been studied extensively. The particle size, impurities of cationic and anionic nature, processing conditions (temperature and pressure) and other external factors (such as the imposition of an electric or magnetic field) are some of the key factors that bring about the irreversible anatase-to-rutile phase transformation. It has been demonstrated that smaller particle size and presence of aliovalent impurities lead to this transformation at lower temperatures.

3.1.2 Titania coating on Ti plate specimen by PED process

The coatings of titania on the plates and mesh were created with different thicknesses by the PED process developed by the Henkel Inc. They were imaged by SEM and analyzed for their gross chemical composition by EDS; the TiO_2-coated plates were also subjected to x-ray diffraction for phase identification. Fig. 8 shows the systematic evolution of the surface morphological features, with increasing thickness of titania coating on the plate samples.

As can be seen, with increasing film thickness, the structure goes gradually from all high aspect (l/d) ratio 1-D fibers, to a mixture of 1-D fibers and 2-D platelets, to 2-D platelets and 3-D rods. Moreover, the surface densification also increases; a thinner titania film is endowed with more nanofeatures and more void space which may allow for higher and direct exposure of the bacterial species with the photoactive surface. On the other hand, the microscale platelets and rods offer a larger surface area, which also could be beneficial in the bacterial necrosis per unit area. The elemental distribution of titanium and oxygen is shown in Fig. 9.

The XRD analysis showed the presence of TiO_2 in rutile phase in all the four samples, as can be seen from Fig. 10. The identical XRD signatures confirm the reproducibility of the PED coating technique developed by Henkel and the uniformity in film growth.

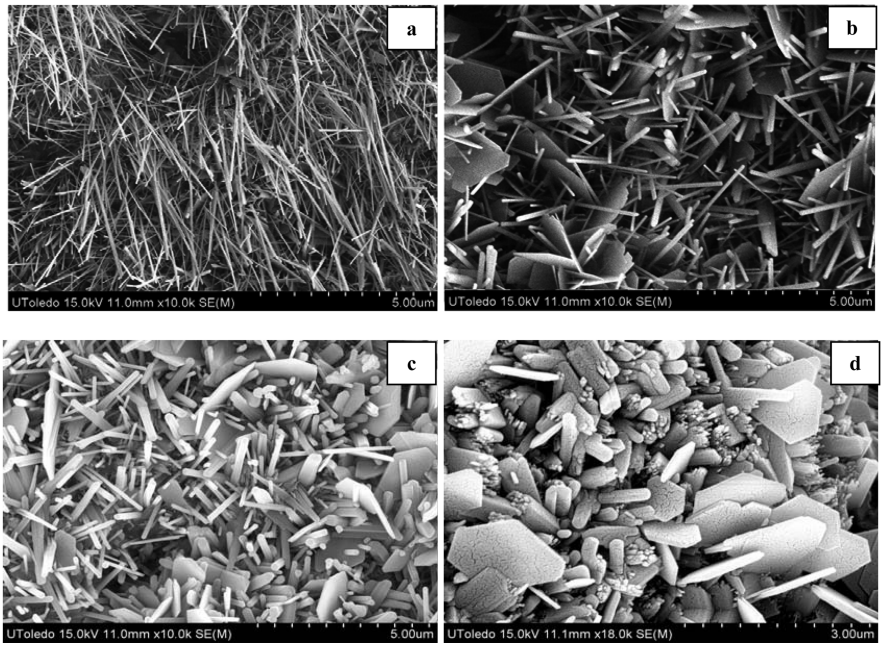

Fig. 8 SEM images of TiO_2-coatings of increasing thickness (a = 1.3 μm, b = 2.4 μm, c = 3.7 μm and d = 5.0 μm) on Ti plates; the PED-coated samples were fired at 800°C for 4 h

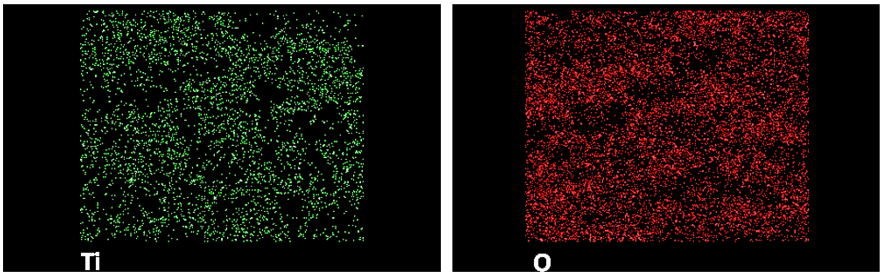

Fig. 9 Elemental mapping of Ti and O on the TiO_2-coated Ti plate

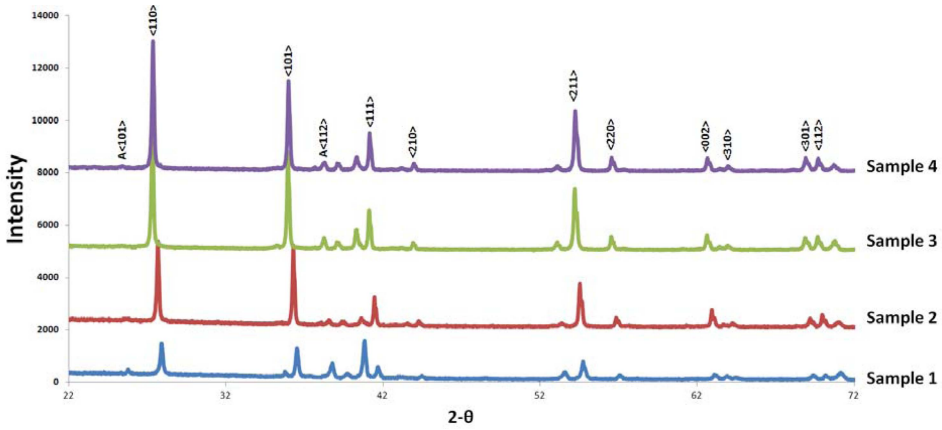

Fig. 10 XRD signatures of the coating on Ti plates after firing at 800°C for 4 h. The diffraction peaks predominantly belong to rutile titania with minor peaks conforming to the anatase (A) modification

3.1.3 Titania coating on Ti mesh specimen by PED process

The morphological features of the titania films deposited on Ti mesh are distinctly different from those on Ti plates, as seen in Fig. 11.

The morphology also changed with increasing coating thickness. Fig. 12 shows morphological variation in the titania films of different thickness formed on the Ti mesh. Fig. 13 shows the

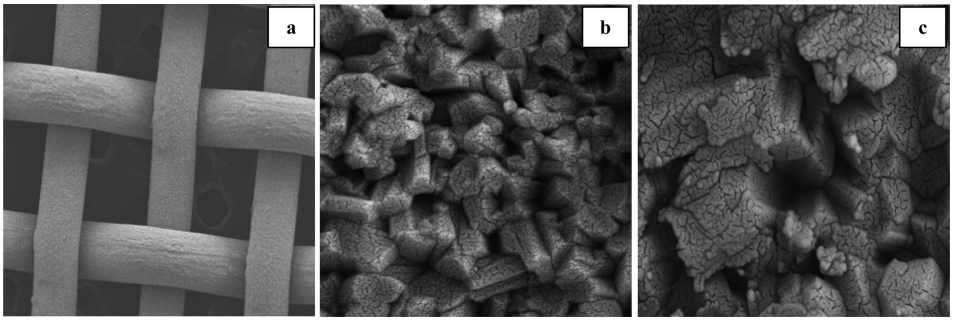

Fig. 11 Morphology of (a) pure Ti-mesh, (b) Henkel TiO_2-coated Ti mesh fired at 800°C for 4 h and (c) is a higher magnification image of coating (b)

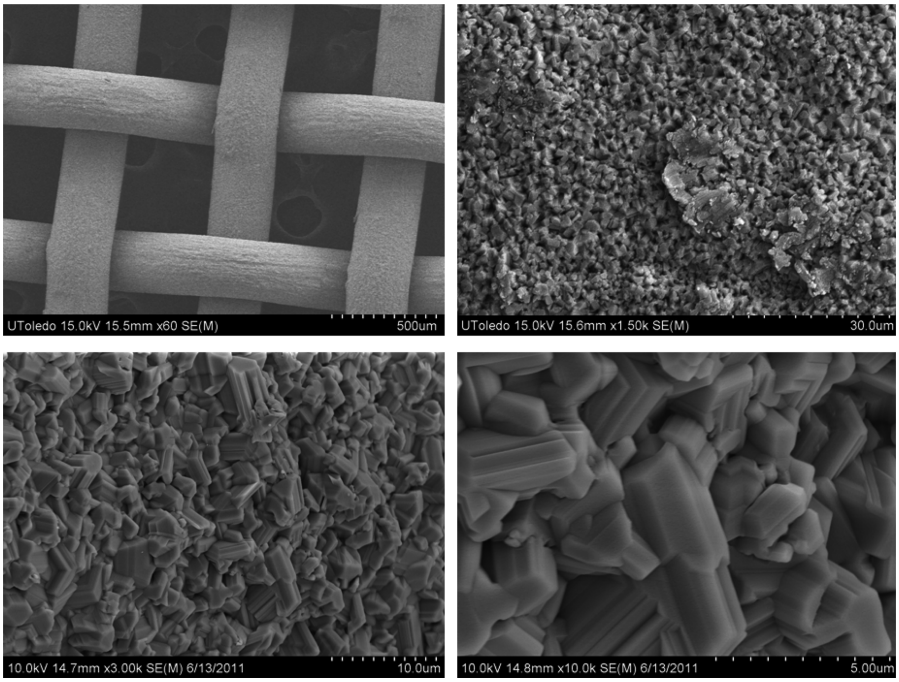

Fig. 12 SEM images of Ti mesh coated with thinner (top-left) and thicker (bottom) TiO_2 films by the PED process

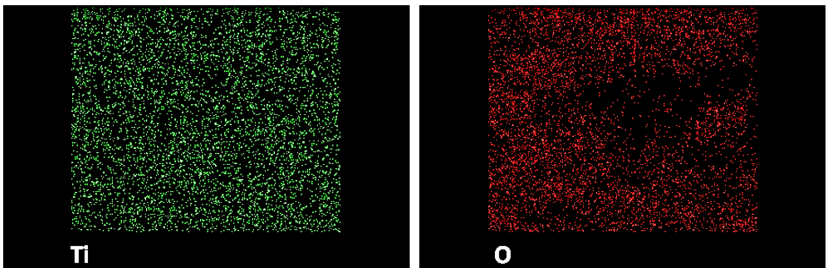

Fig. 13 Elemental mapping of Ti and O on the TiO_2-coated Ti mesh

elemental dispersion of titanium and oxygen across the sample surface, indicating the formation of uniform TiO_2 coating on the Ti surface.

Fig. 14 shows the systematic variation in the thickness of TiO_2 film coated by PED process on mesh samples. The film thickness increases monotonically and almost linearly, which is also corroborated by the SEM images of the successive films, taken at same magnification (inset).

A similar trend was observed in the case of plates as well, but is not shown here to avoid redundancy.

Theoretically, a film of stoichiometric TiO_2 contains 60 *wt*.% (33 at.%) of Ti and 40 *wt*.% (67 at.%) of O. The EDS analysis (accuracy limit ±3%) of mesh and plate specimens presented in Table 2 shows that the target compound, viz., TiO_2, was formed in the films, which confirms the XRD results.

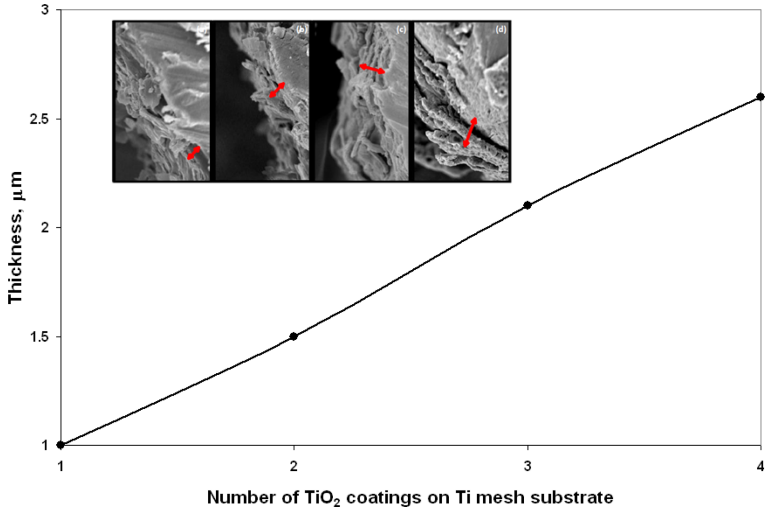

Fig. 14 Variation in the thickness of TiO_2 coating on Ti mesh. Inset: SEM images of TiO_2-Ti cross-sectional interface for sample with varying titania film thickness (red arrow is a measure of the thickness of titania film on the Ti substrate)

Table 2 EDS elemental composition of TiO_2-coated mesh and plates

Sample	TiO_2-coated Ti mesh		TiO_2-coated Ti plate	
Element	*wt*%	at%	at%	at%
Oxygen (O)	36.74	63.49	40.94	67.48
Titanium (Ti)	63.26	36.51	50.06	32.52

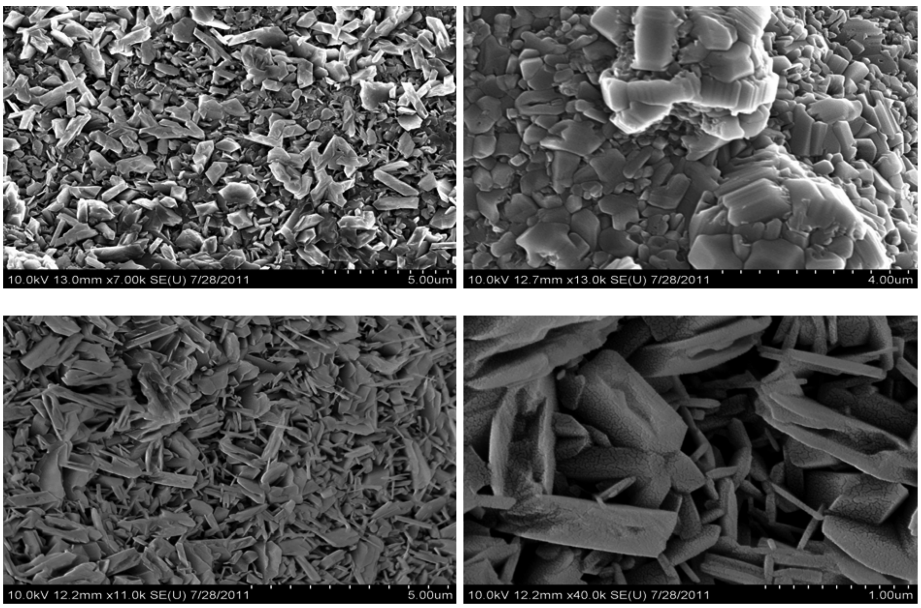

Fig. 15 SEM images of the TiO_2-coating on Ti6Al4V rod specimen

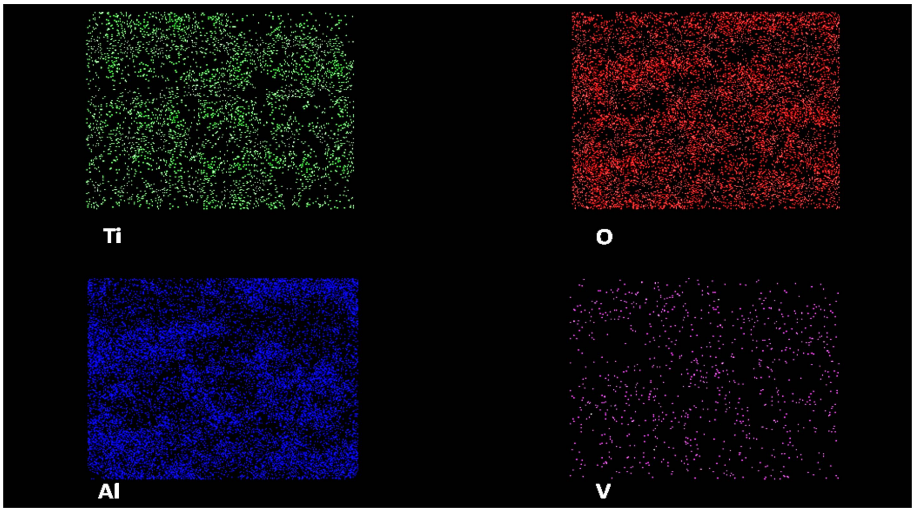

Fig. 16 Elemental mapping of the TiO_2-coated Ti6Al4V rod specimen

Table 3 Elemental composition of TiO_2-coated Ti6Al4V rods

Sample	TiO_2-coated Ti6Al4V rod (inclusive of all elements)		TiO_2-coated Ti6Al4V rod (only Ti and O)	
Element	*wt*%	at%	*wt*%	at%
Oxygen (O)	28.19	52.74	36.74	63.49
Titanium (Ti)	64.99	40.61	63.26	36.51
Aluminum (Al)	5.06	5.62	-	-
Vanadium (V)	1.76	1.03	-	-

3.1.4 Titania coating on Ti6Al4V rod specimen by PED process

The PED coating process applied to the Ti6Al4V alloy rods also created uniform layers of titania, albeit with morphologies somewhat distinct and subtle from what were seen on the plates. These morphological and compositional differences could be attributed to the nature of the substrate; in the case of rod samples, the chemical interaction would be affected by the presence of Al and V. Fig. 15 shows the SEM images of the titania coating on Ti6Al4V rods.

EDS analysis was conducted on the pristine alloy as well as on the coating; the latter is presented in Fig. 16 which indentifies all the elements present in the sample in uniform distribution across the specimen relative to their fraction in the alloy. Discounting the presence of aluminum and vanadium in the coating, the atomic ratio of 1:2 for Ti to O is obtained, as shown in Table 3.

3.1.5 Titania coating on mesh by anodization

Anodization created completely different morphology. As seen in the SEM images shown in Fig. 17, titania in a nanotubular surface structure was formed on the mesh substrate. Large population of nanotubes endows a vast surface area.

The average outer (OD) and inner diameter (ID) of the nanotubes was 171 nm and 113 nm,

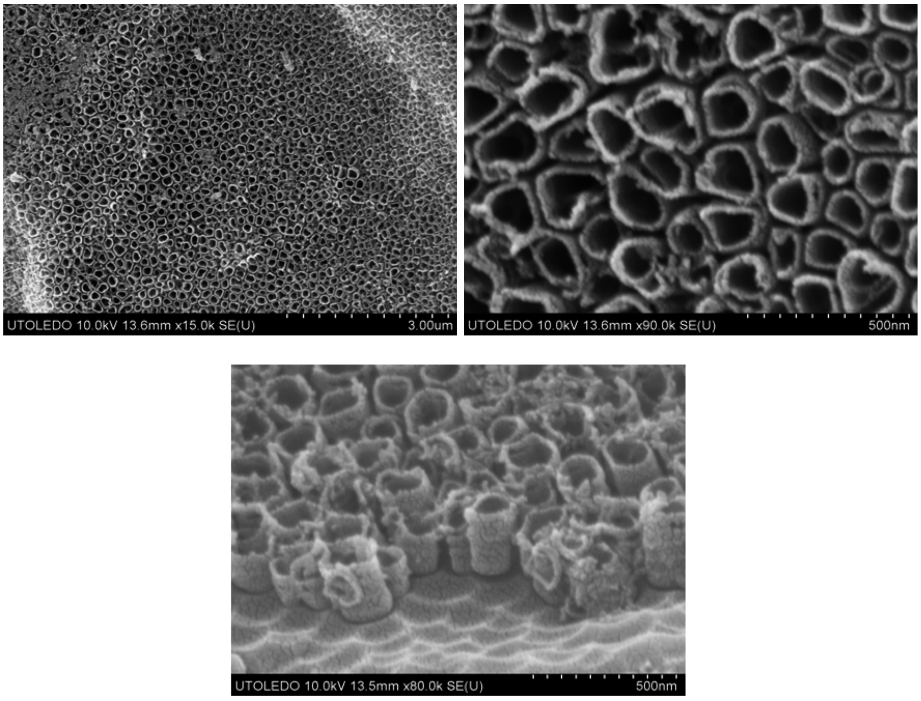

Fig. 17 SEM images of TiO_2 nanotubes formed on Ti mesh by anodization for 30 min. at 21 V in a HF + H_3PO_4 mixture

Table 4 Elemental analysis of the anodized Ti mesh

Sample	As-anodized Ti mesh		Heat-treated anodized Ti mesh	
Element	*wt*%	at%	*wt*%	at%
Oxygen (O)	18.43	40.35	25.31	65.77
Titanium (Ti)	81.57	59.65	74.69	34.23

respectively. Thus, anodization is capable of creating very small tubular structures within a short period of time (1/2 h). Interestingly, the Ti:O ratio in the as-formed nanotubes was somewhat higher. However, heating the anodized specimen in a profile, used in the case of Ti and Ti6Al4V specimen coated by PED process, lowered the ratio to the expected level. This is shown in Table 4.

3.2 Evaluation of bactericidal efficacy of photoactivated titania

With the aid of the Invitrogen live/dead assay, the cell necrosis was followed in real time and still images were taken at different intervals, starting from the time of activation (t = 0 min.) to 40 min.; the activation was caused by irradiation with a hand-held IR laser device (λ = 808 nm). Fig. 18 shows time-lapse shots of an *S. aureus* suspension not exposed to either photoactive titania nanomats or the IR radiation, over a period of 20 minutes. This constituted the control experiment and demonstrates the complementary function of the photoactivating substrate and radiation source

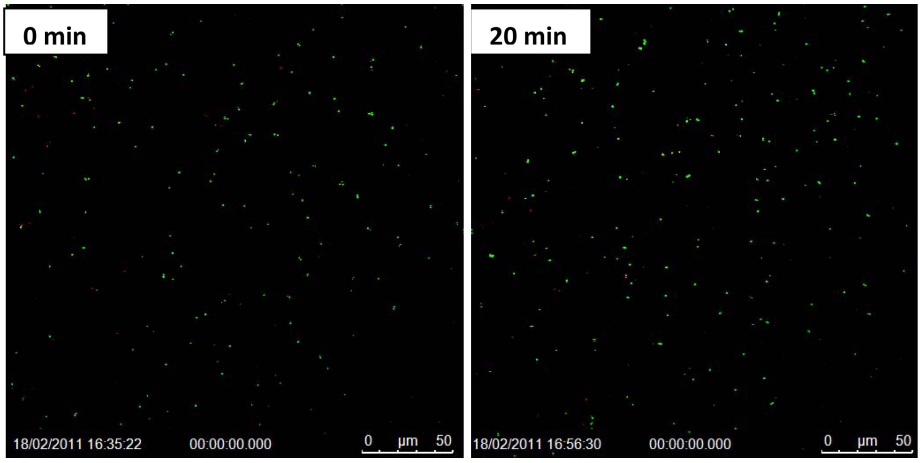

Fig. 18 Confocal images of control experiment with *S. aureus* suspension without titania or IR radiation (green/SYTO9 = live cells; red/PI = dead cells)

to cause the desired necrosis. This protocol was designed to prove that a combination of titania (photoactive agent) and IR (photon source) both is needed to induce the desired bactericidal effect. This is borne out of the fact that although any source of radiation over an extended period of time, might create an unfavorable environment for the bacteria, the efficiency of a bactericidal event requires a radiation source and a photoactive precursor to be present. In all the confocal images, green pixels (SYTO9) identify live cells and dead cells are recognized by red pixels (PI). For quantification of bacterial necrosis/survival, the cells were counted individually at the two time intervals. For this, the still-shots taken during time-lapse imaging were uploaded into the ImageJ software and configured in order for all cells to be visible and countable.

3.2.1 S. aureus necrosis by TiO_2 nanofibers

The bactericidal efficacy of pure and doped titania nanofibers towards *S. aureus* upon IR activation is shown in Figs. 19 through 21 in terms of the progress of cell necrosis over time. Interestingly, pure TiO_2 nanofibers showed accelerated necrosis potency, with a significant drop in the bacterial viability within a short span of time lapse. The image captured at zero time shows almost 100% of the cells surviving. The count indicates that within 10 min. almost 90% of these are engulfed by the PI stain, indicating damaged membranes due to cell death; at the end of 10 min., only 12.8% survive and at the end of 30 min. period, only 2.5% cells survived.

The confocal images with the live/dead assay for Fe-doped titania nanofibers in *S. aureus* suspension are shown in Fig. 20, which clearly shows the photoactivation-mediated bactericidal attributes of the Fe-doped TiO_2 fibers.

In this case, bacterial necrosis at a slower pace was observed. The Fe-doped samples showed only 60% decay of the *S. aureus* microorganism within the first 10 min. after IR exposure. Even after a lapse of 30 min., the PI continues to actively penetrate the diaphragm of the *S. aureus* cells which were still viable since the time of photactivation. The bactericidal efficacy of the Fe-doped fibers also approached 90%, with approximately 13.4% of the cells surviving after 30 min. of exposure, as seen from Fig. 20.

Similar effect was seen in the bactericidal potency of Ag-doped nanofibers too. The 1 *wt*% Ag-

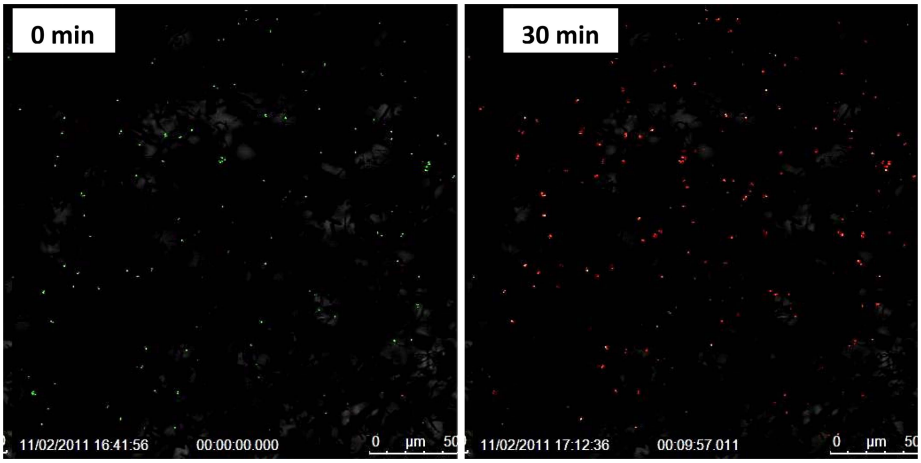

Fig. 19 Confocal images of bacterial colonies at different times after activation of pure TiO_2 fibers dispersed in *S. aureus* broth by IR laser for 30 s (green/SYTO9 = live cells; red/PI = dead cells)

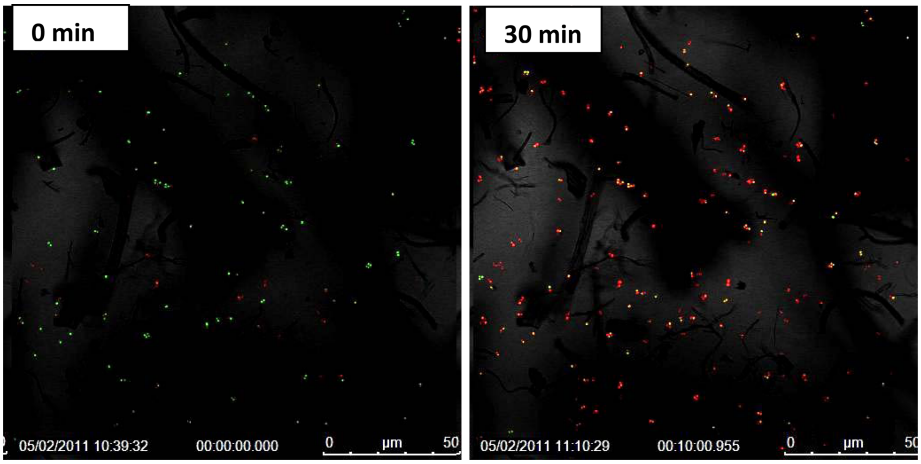

Fig. 20 Confocal images of the bacterial colonies in Fe-doped TiO_2 nanofiber suspension in *S. aureus* broth at different times after activation by IR laser for 30 s (green/SYTO9 = live cells; red/PI = dead cells)

doped TiO_2 formulation showed high cell necrosis (Fig. 21).

However, silver-doping did yield better results compared to its iron counterpart, but still did not exceed the superior performance of pure titania fibers, with only 12.2% and 8.9% cells surviving after 10 and 30 min., respectively, from exposure. Even though the survival rate at the end of 30 min. was quite low, it should be mentioned that the Ag-doped fibers caused necrosis of cells within as little as 10 min. with the survival rate only decreasing by 3.3% between 10 to 30 min., whereas, the pure titania fibers created a decrease of over 10.3% between these two time points.

Although the cell necrosis was seen throughout the entire bacterial suspension in all the three cases of electrospun nanofibers, it was observed more prominently in the area where the activated fibers were placed, and even more specifically where the IR laser beam was most centralized and concentrated. It was this area where the time lapse imaging was concentrated for 30 min. from the

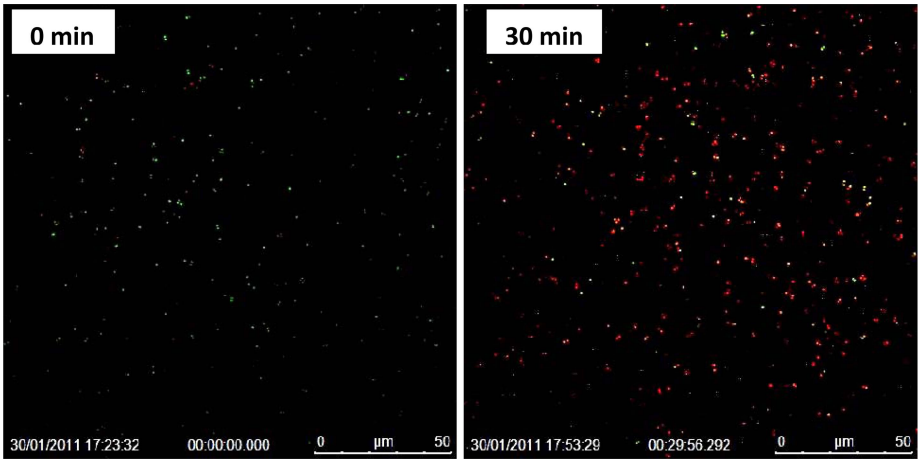

Fig. 21 Confocal images of the bacterial colonies in Ag-doped TiO_2 nanofiber suspension in *S. aureus* broth at different times after activation by IR laser for 30 s (green/SYTO9 = live cells; red/PI = dead cells)

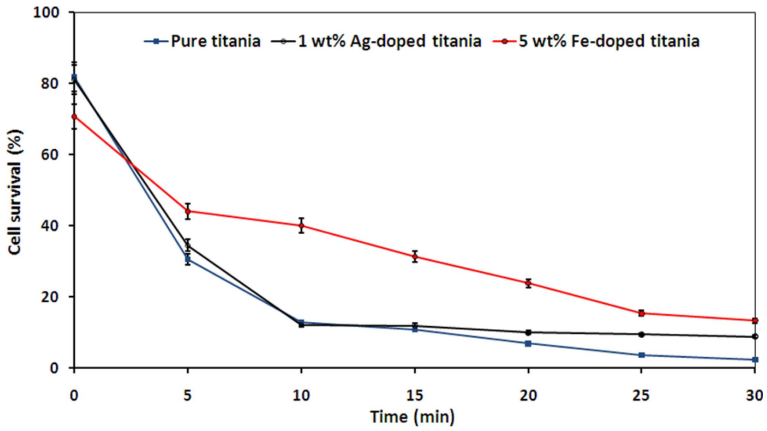

Fig. 22 Time-dependent decay of the bacterial colonies in the presence of pure and Ag- and Fe-doped TiO_2 nanofibers suspended in *S. aureus* broth after activation by IR laser for 30 s

time of activation (t = 0 min.). The variation seen in the number of cells at different imaging time intervals is a result of cells moving in and out of the plane that is being imaged.

It is expected that the addition of dopants would increase the bactericidal efficacy of the nanofibers upon photoactivation. The advantage of one dopant over the other was not hypothesized because both Fe and Ag are known to possess excellent antibacterial properties. The results showed that Fe-doped fibers needed somewhat longer time to obtain efficacy comparable to that of pure and/or Ag-doped TiO_2 fibers. The observed discrepancy could be ascribed to a number of factors. For example, it is likely that fibers were more concentrated in one location during one test as opposed to the other (a not easily controllable experimental artifact). This would cause greater/quicker necrosis in one instance compared to other. Furthermore, although the dopants such as those employed here are well known for their antibacterial properties, they may not be necessarily photoactive, which is the main driving force in the necrosis mechanism implemented here.

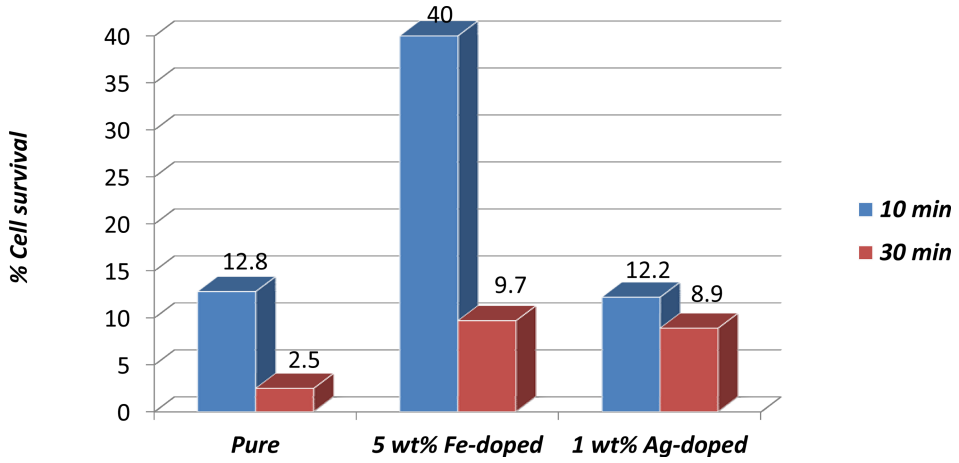

Fig. 23 Fraction of the surviving *S. aureus* cells after 10 and 30 min. from IR activation of pure, Fe- and Ag-doped TiO_2 nanofibers

Therefore, it is likely that adding or increasing the doping concentration would limit the bactericidal attributes of the pristine fibers. However, the precise mechanism and the difference in the performance of the doped counterparts of pure titania is not well understood at this time. More systematic studies are required to elucidate the precise role of the dopant towards bactericidal activities. The systematic variation in the cell survival rate as a function of time after irradiation by IR laser for 30 s is shown in Fig. 22, which clearly brings out the superiority of pure titania over its doped analogs.

This aspect is amplified further in Fig. 23 which compares the % surviving cells at two relevant time points.

3.2.2 S. aureus necrosis by TiO_2-coated Ti mesh and plates

We have previously reported the fabrication of titania coatings by anodization, hydrothermal processing and the PED technique. Their bactericidal efficacy against *E. coli* was also successfully demonstrated. Activation by IR laser (λ = 808 nm) for 30 s proved effective in the necrosis of *E. coli* cells up to 40%. The photocatalytic response of free-standing titania in other formats (powder, nanofibers, etc.) in the presence of UV radiations has also been reported (Azad *et al*. 2011, Azad *et al*. 2010, Koseki *et al*. 2009, Yu *et al*. 2003, Oka *et al*. 2008).

The UV radiations (λ = 365 nm) employed hitherto are of lower intensity though of larger photon energy (de Broglie's equation of wave length-energy equivalence: $E = hc/\lambda$; where h is Planck's constant, c the speed of light and λ the radiation wave length). Consequently, longer exposure time (reaching 60 min. to 2 h in some cases) is needed to obtain significant results. On the other hand, the IR laser source used by the present authors in this as well as previous work, is of larger wave lengths, and hence of smaller photon energy. However, these laser beams are of much higher source intensity (1 W/cm^2). This effectively creates a larger population of incident photons per unit area and it is this parameter that functions as a deciding factor in the observed photoactivation-mediated effect in the cell necrosis. A larger photon flux (number per unit incident area) in the case of IR source as opposed to UV source is likely the reason for observed agile and more quantitative bactericidal activities in relatively shorter span of time on the titania surfaces. A shorter exposure

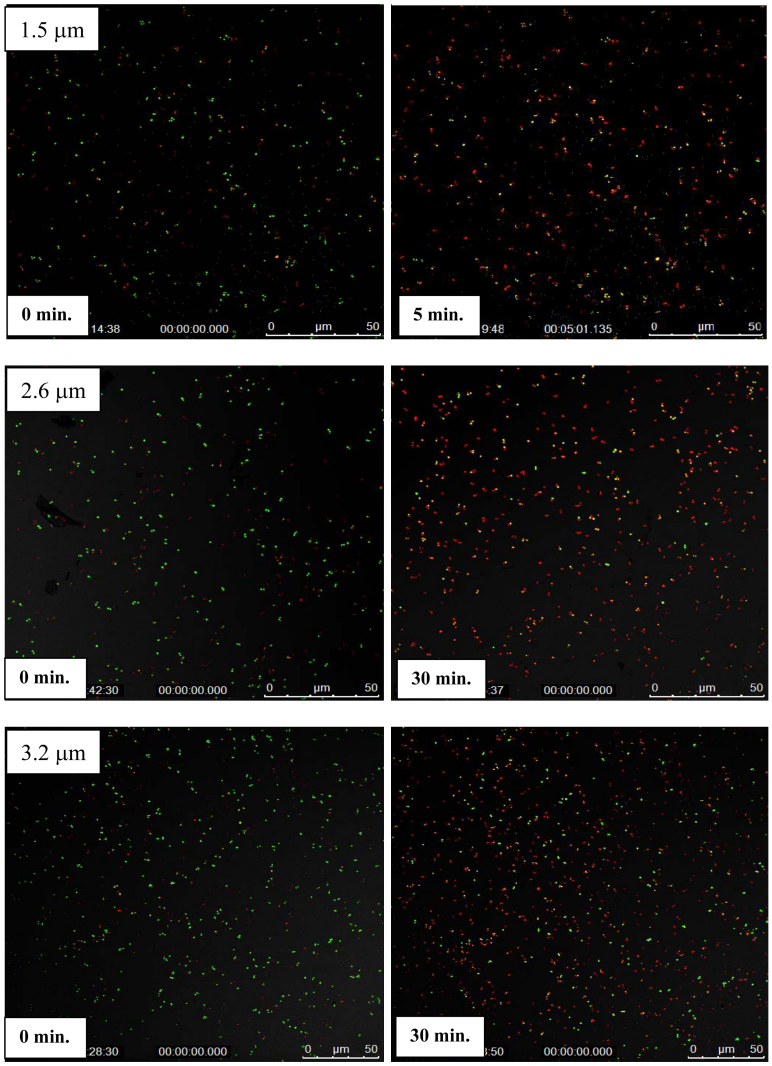

Fig. 24 Confocal images of the bacterial colonies at different times in *S. aureus* suspension containing Henkel TiO_2-coated mesh samples fired at 800°C/4 h and exposed to an IR laser for 30 s (green/SYTO9 = live cells; red/PI = dead cells)

would limit the time the patient is exposed to radiations, thereby making the effectiveness of the technique more attractive and applicable for clinical applications. Furthermore, in the light of the fact that longer exposure to UV radiation (up to 60 min. or more) does not induce quantitative necrosis, repeated exposures would be needed. Under these conditions, one might reach dose levels that are harmful to human tissues.

This explanation corroborates the brief but effective use of an IR source and strengthens the following results obtained on the titania-coated plate and mesh samples; to the best of our knowledge no such data exists with a parallel study using UV activation by others.

The titania-coated plate and mesh samples were evaluated for their antibacterial efficacy against *S.*

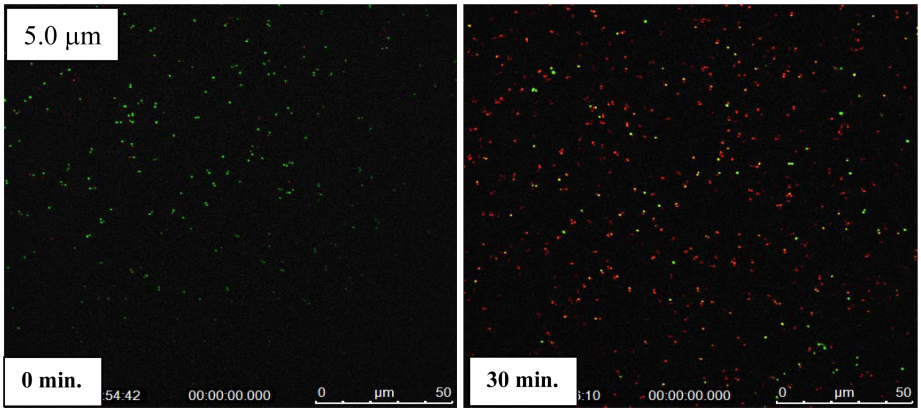

Fig. 25 Confocal images of the bacterial colonies at different times in *S. aureus* suspension containing Henkel TiO_2-coated plate sample (fired at 800ºC/4 h) and exposed to an IR laser for 30 s (green/SYTO9 = live cells; red/PI = dead cells)

aureus. Confocal imaging using SYTO9 and PI stains was employed to monitor the status of bacterial cells as a function of time after sample irradiation of the sample and its immersion in the microbial bath. A Ti mesh coupon with a 1.5 μm thick TiO_2 coating was subjected to IR activation for 30 s followed by immersion in a bacterial suspension of stained *S. aureus* cells. The specimen was placed as to expose the bacteria to the photoactivated region of the mesh. Confocal imaging was recorded in real-time as the bactericidal effects of the titania coating took effect. Fig. 24 illustrates the quick effect of the Henkel-coated mesh in causing *S. aureus* cell necrosis. Within approximately 5 min. of exposure, only 23.71% of the *S. aureus* cells survived; the concentration of the surviving cells was 9% after 30 min.

A note of clarification with regard to the time stamp of 0 min. on the confocal images is warranted. The images marked as '0 min.' were realistically taken a few moments after actual exposure to the titania-coated mesh due to the time elapsed between activation and placement in the suspension, before being placed inside the slide holder of the apparatus. An additional amount of time also elapsed in positioning the center of the microscopic lens on the activated area prior to imaging. This would explain the observed cell necrosis already taken place at 0 min. in some of the images.

Fig. 24 also shows the bactericidal efficacy of the mesh samples with titania coating thicknesses of 2.6 μm and 3.2 μm. Although these mesh samples did cause evident cell necrosis, they were not found to be as effective as the sample with a smaller coating thickness. The survival count after 5 min. of exposure was 50.7% for sample 4, which dropped down to 21.5% after a time-lapse of 30 min. In comparison to sample with a thinner titania coating (1.5 μm), the cell survival concentration was slightly more than twice on sample with 2.6 μm thick titania coating. Increasing the coating thickness of the Ti mesh to 3.2 μm did increase the bactericidal efficacy as compared to that with 2.6 μm thick coating by 10% after only 5 min. However, the cell survival for this sample was approximately 22.3% after 30 min. This is slightly less effective but portrays relatively equivalent results.

The bactericidal efficacy of Ti plates was also tested against *S. aureus*. It was found that coated mesh samples were more effective because of their more immediate access to the bacterial

Table 5 Summary of the efficacy of the TiO_2-coated mesh and plate samples activated by IR laser for 30 s in *S. aureus* suspensions. The data represent an average of 10 measurements with each of the mesh and plate samples and has an uncertainty of ±2%

Material	Titania film thickness	Post-exposure cell survival (%) after a time-lapse of	
		5 min.	30 min.
Control (no exposure to TiO_2/IR)	-	100	100
TiO_2-coated Ti mesh	1.5 μm	23.7	9.0
TiO_2-coated Ti mesh	2.6 μm	50.7	21.5
TiO_2-coated Ti mesh	3.2 μm	42.6	22.3
TiO_2-coated Ti plate	5.0 μm	55.7	12.9

suspension as is apparent by the structural difference between plates and mesh. Therefore, cell necrosis was apparently detected in one Henkel-coated plate sample of thickness 5 μm, the results of which are seen in Fig. 25.

It should be noted here that placement of the plates among the bacterial suspension incorporated a further degree of difficulty because of the dense and bulky nature of the material. It was necessary for the plate to be fully exposed to the *S. aureus* cells while not "crushing" the cells or distorting bacterial movement, which therefore leads to distortion of the fluorescent imaging by confocal microscopy. For this reason, bactericidal efficacy of the Henkel-coated plates was not consistent throughout. Still, the results for Henkel-coated plate showed its successful antibacterial effect against *S. aureus,* indicating that only 55.7% of cells survived after 5 min.; the survival diminished to about 12.9% after 30 min. The data is summarized in Table 5, and shown graphically in Fig. 26.

From the data sown in Table 5, it can be concluded that titania-coated Ti mesh samples had an increased efficacy towards cell necrosis as compared to Ti plates. This increased effect can be attributed to the ability of mesh to be more accessible to the bacterial suspension because of its porous structure. In addition, thinner coatings were more effective in causing necrosis of the bacterial cells. Ti plates and mesh with increasing coating thicknesses caused slightly lower cell death after activation, though still comparable with the highest survival count being around 20%.

At first sight, these results might appear counterintuitive, but the increased efficacy observed in this study can be explained as a combination of a number of factors related mainly to the structural artifacts of the coating. For example, the particle density of TiO_2 is much greater in thinner coatings, thus allowing for more titania particles packing within a unit space. Second, there is a gradual but definite change in shape and particle distribution between thin and thick coatings. This results in a corresponding change in the aspect ratio (length to diameter; *l/d*) as seen clearly from the SEM images shown earlier. The effectiveness of the thinner film (with larger aspect ratio) is therefore due to the availability of larger surface area on the thinner coating within the contour of limited activation area of the laser beam.

This behavior of titania coatings could be used for the implant activation in both pre and post-surgery situations. In post-surgery cases, this may simplify the reactivation step if the infection

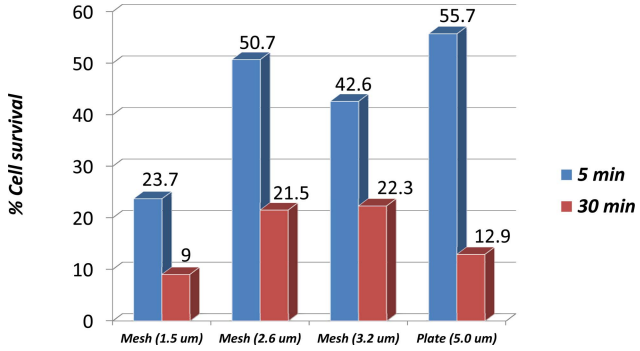

Fig. 26 Fraction of the surviving *S. aureus* cells after 5 and 30 min. from IR activation of TiO_2-coated mesh and plates

persists after surgery. Furthermore, IR radiations are capable of penetrating skin and other soft tissue, which might necessitate little or no surgical incision. Currently, the persistence of surgical site infection often requires re-opening and removal of implants for ex-vivo sterilization and even replacement in some cases. With a titania pre-coated implant in place, that could be activated and re-activated as required, the necessity of additional surgical procedures would potentially diminish.

3.2.3 S. aureus necrosis by TiO_2-coated Ti6Al4V rods

The successful demonstration of the effect of TiO_2-coatings on Ti mesh and plates in causing *S. aureus* cell necrosis prompted the implementation of a more clinically relevant Ti substrate. Thus, we proceeded to employ Ti6Al4V alloy material which is widely used in prosthetic devices due to its excellent implantable stability. Spinal rods made of Ti6Al4V were coated with TiO_2 by PED process and tested against *S. aureus* with slight change of protocol. Here, the radiation-mediated activation was performed after placing the titania-coated rod sample in the *S. aureus* suspension. This simultaneous activation allowed for a direct comparison of the results with those with pre-activation.

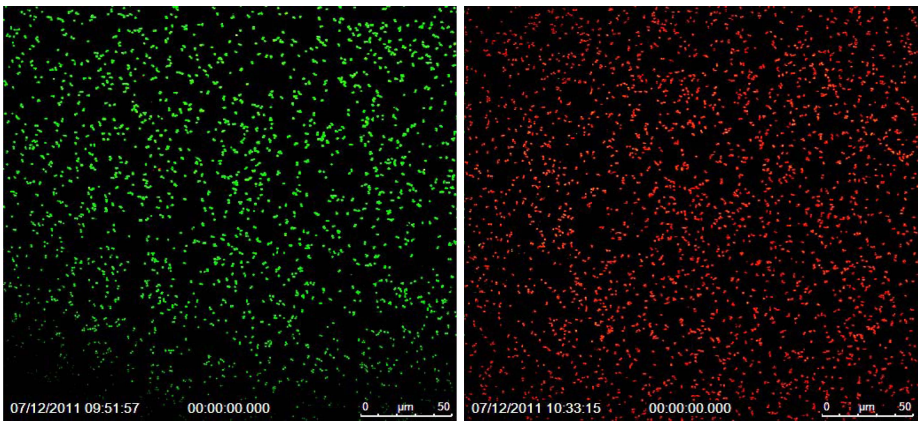

Fig. 27 Confocal images of bacterial colonies with the TiO_2-coated Ti6Al4V rod submerged in *S. aureus* suspension and activated simultaneously by IR laser for 30 s. Left image is before and the right immediately after exposure (green/SYTO9 = live cells; red/PI = dead cells)

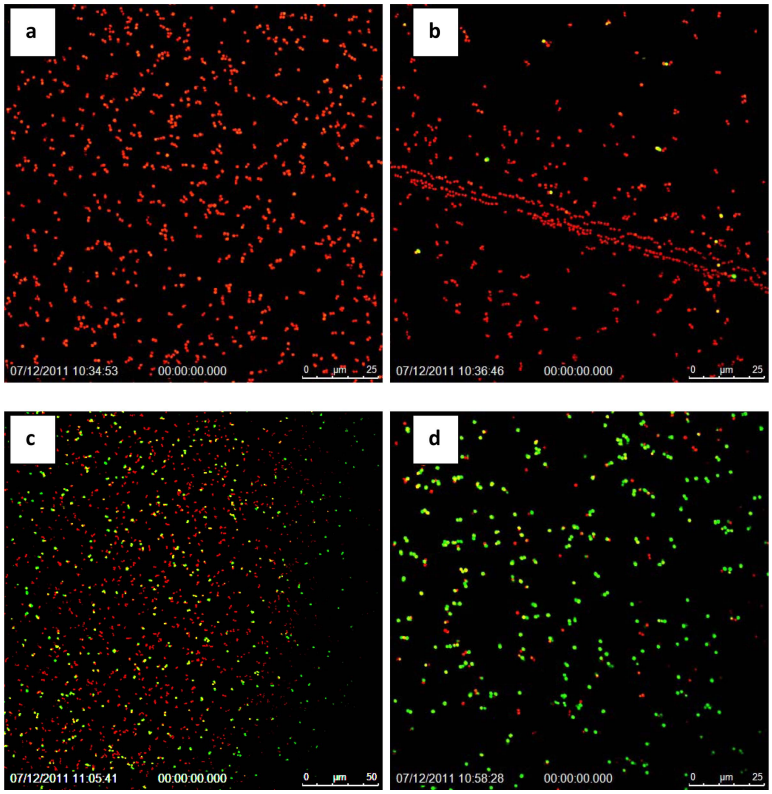

Fig. 28 Confocal images of the bacterial colonies with the TiO_2-coated Ti6Al4V rod sample submerged in *S. aureus* suspension and activated simultaneously by IR laser for 30 s: (a) immediately under rod surface, (b) near the circumference that is in contact with the broth, (c) near the circumference that is partially in contact with the broth and (d) at a location away from the rod (green/SYTO9 = live cells; red/PI = dead cells)

Confocal imaging was obtained after the implant sample was activated by IR laser for 30 s, while submerged in the bacterial suspension. It was found (Fig. 27) that simultaneous activation caused effectively 100% bacterial cell necrosis, within a short span of time (almost immediately) upon activation, highlighting the superiority of this modified method of activation as compared to that employed in the case the mesh/plate samples, discussed earlier.

These results are reminiscent of those obtained with nanofiber samples, where they were also activated simultaneously, with the bacterial suspension, after they were submerged in the broth. The main difference between the two cases, however, is that the dispersion of fibers in suspension created somewhat lower degree of bactericidal efficacy as compared to the rods. A comparison of the images shown in Fig. 27 with those in Figs. 19 through 21, illustrates this point elegantly.

Yet, in comparison to the titania fibers and titnia-coated mesh and plates, the overall bactericidal efficacy of rod samples is not uniform. This is borne out of the inherent limitation associated with the ‘area of reach’; in the latter case, this ‘area of reach’ is not uniform. The cell necrosis in all experiments was seen mainly within the area directly exposed to the materials, whether fibers, mesh, plates or rods. This is evident from Fig. 28.

The ability to reactivate a single titania-coated rod sample for multiple uses was also examined.

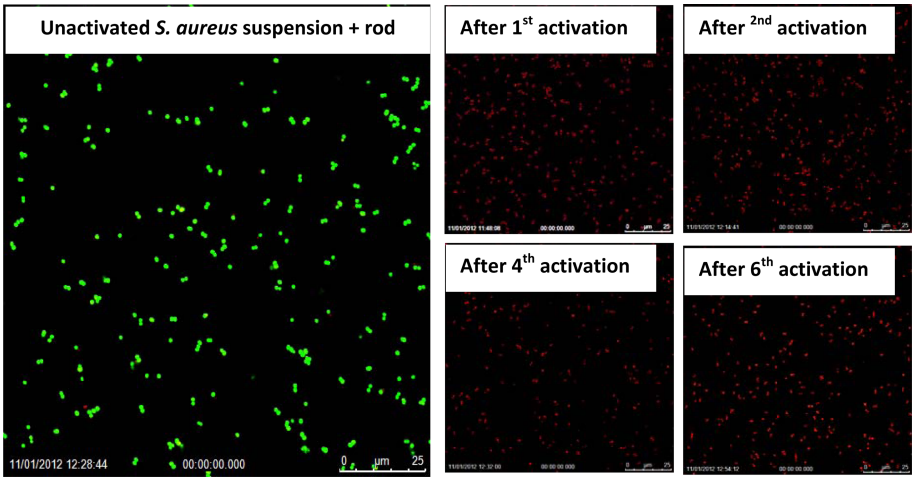

Fig. 29 Confocal images showing the effectiveness of TiO_2-coated Ti6Al4V rod specimen submerged in fresh *S. aureus* suspensions simultaneously and repeatedly activated by IR laser for 30 s (green/SYTO9 = live cells; red/PI = dead cells)

For this purpose, one used rod specimen with titania coating was rinsed with DI water, placed in a fresh *S. aureus* suspension and activated again with 30 s IR exposure. This was repeated up to 10 times using fresh bacterial suspension each time. Confocal images were taken both before and after the exposure. The results are shown in Fig. 29.

The sustained bactericidal propensity in repeatedly activated TiO_2 coatings was thus verified, with no measurable sign of deterioration. Also, nearly 100% necrosis was achieved after every activation procedure. Additionally, the implementation of fine point IR laser needles could aid in the extension of this technique to achieve promising results in in-vivo studies, thus opening new clinical premises that allow IR radiation to penetrate skin and reach the coated prosthetic materials.

As stated in the Introduction section, studies on photoactive/antibacterial efficacy of titania (as powder, thin film coating ornanofibers) have been reported in the literature. However, the use of infrared (IR) radiation as the activation source has not been reported; our studies showed the superiority of IR over ultraviolet (UV) source of activation, as well as the advantage of an IR laser as compared to an IR flashlight (Azad *et al*. 2010, Azad *et al*. 2011, Hershey 2010). In this connection, relating the bactericidal effect, a study by Azad *et al*. (2010) using pure and Fe-doped titania nanofibers demonstrated the advantage of photoactivation of these fibers with an IR (λ = 830 nm) activation for 12 s over UV (λ = 350 nm) activation for 20 min. Moreover, no previous work had shown such an immediate bactericidal effect with 100% cell necrosis.

Another study tested the bactericidal efficacy of TiO_2 particles against *S. aureus* under UV and fluorescent light activation (Koseki *et al*. 2009). Though, effective bacterial necrosis (exceeding 90% with UV) was demonstrated, it required exposure for 1 h; there were only 10.9% live cells with fluorescent exposure. Long exposure is not practical in clinical applications, where lengthier exposure of a wound or surgical site might increase the risk of further complications.

Yu *et al*. (2003) have reported the fabrication of Fe-doped TiO_2 films on stainless steel substrates by dip coating followed by calcination and their use as antibacterial agent for sterilization against *Bacillus pumilus*. In this case, a suspension of *Bacillus pumilus* was placed onto the TiO_2-coated

Table 6 Comparison of representative results of present study with the literature

Material (TiO_2)	Exposure time	Light source	Photon/Area‡	Survival rate (%)	Reference
Pure nanofibers	30 s	IR (λ=808 nm, 1 W/cm^2)	6.1×10^{20}	2.5	This work
Ti mesh (pre-activation)	30 s	IR (λ=808 nm, 1 W/cm^2)	6.1×10^{20}	9.0	This work
Ti rods/mesh (simultaneous activation)	30 s	IR (λ=808 nm, 1 W/cm^2)	6.1×10^{20}	0	This work
Powder	60 min.	UV (λ=352 nm, 1.8 mW/cm^2)	1.2×10^{19}	9.4	Koseki *et al.* (2009)
Powder	60 min.	Fluorescent (λ=352 nm, 0.8 mW/cm^2)	5.1×10^{17}	10.9	Koseki *et al.* (2009)
Film on substrate	120 min.	UV (λ=365 nm, 630 mW/cm^2)	8.3×10^{18}	50	Yu *et al.* (2003)
Powder	60 min.	UVA (λ=365 nm, 1.1 mW/cm^2)	7.3×10^{18}	7	Oka *et al.* (2008)
ZnO/TiO_2 nanocomposite	30 s	UV (λ=312 nm, 6 W/cm^2)	2.8×10^{20}	13.3	Huang *et al.* (2011)

‡Incident photons per unit area integrated over the exposure time; it is obtained by multiplying the ratio of the source intensity (W/cm^2) and photon energy (J) with the time of exposure (s)

stainless steel plate that was irradiated by a UV lamp (intensity rating 630 mW/cm^2; λ = 365 nm). Their results showed that the active *Bacillus pumilus* colonies on the titania films subjected to UV illumination decreased by 50% after 2 h of exposure. In a recent work, Oka *et al*. (2008) studied the inhibition of bacterial colonization of methicillin-resistant *Staphylococcus aureus* (MRSA) suspensions on TiO_2 photocatalytic film prepared by direct oxidization of pure titanium substrate. In this case, the titania coating on Ti was created by etching the latter with 5–10% HF solution followed by soaking in aqueous H_2O_2 for 2 days. The MRSA suspension on the implant was exposed to the ultraviolet A (UVA) light for 60 min, and the number of colonizing bacteria was estimated. The bactericidal ability of the photocatalyst became apparent after 60 min, when the bacteria had almost disappeared; only about 7% bacteria were found alive. The number of colonizing bacteria on photocatalytic pins also decreased significantly in vivo as well. The titania film was found to be quite effective even against resistant bacterial colonization. In comparison, the technique described here as simultaneous activation attained 0% cell survival with 30 s exposure.

A similar study was reported by Huang *et al*. (2011) using ZnO/TiO_2 nanocomposite and UV source. It was concluded that due to the addition of ZnO, the number of surviving cells decreased to 13.3% with only 30 s of UV exposure, compared to 45% with titania alone.

Table 6 summarizes the results of the present work and compares them with those reported on biocidal efficacy of titania powder, using UV radiation and other types of microorganisms.

In the light of foregoing discussion, the most notable advantage advocated here is the use of IR activation, which has proven to be more efficient in causing bacterial necrosis. Also, simultaneous activation proved most effective.

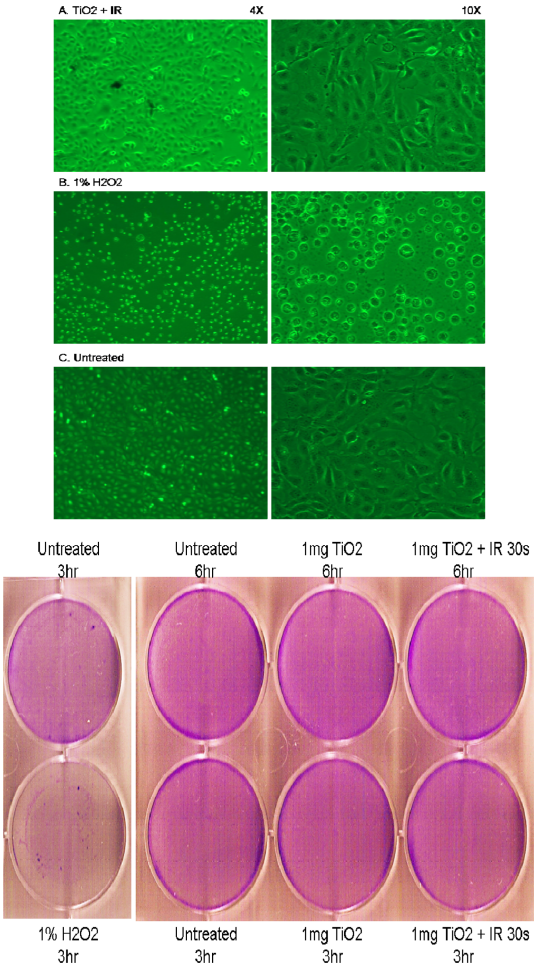

Fig. 30 Benign effect of IR-activated TiO_2 on human A375 cells (left) and mouse embryonic fibroblasts (right)

In addition, the use of IR with an activation time of 30 s is more practical in clinical studies, where greater patient comfort, decreased procedure length and the use of minimally invasive procedures are the sought-after characteristics. With technological advancements, viability of non-invasive activation is very tangible. Also, the reported ability of IR to penetrate skin may potentially allow for more simple activation procedures. Other activation methods using visible light show some merit, but have not yet been tested on bacterial species.

A toxicity study of nanostructured titaniafibers towards tissue cells in human and mouse was carried out by Lin *et al*. (2011) to ascertain if any cell death, inflammatory response or increased regulation in toxic molecules was induced. The prospect of cell death in human A375 cells and mouse embryonic fibroblasts (MEF) was tested by comparing the untreated cells to those exposed to TiO_2 nanofibers activated by IR radiation for 30 s. Comparison was also made with the cells treated with 1% hydrogen peroxide (H_2O_2), which is known to cause cell death.

The results of this investigation are shown in Fig. 30, which illustrate that as compared to H_2O_2 treatment, exposure to photoactivated titania nanofibers was benign; H_2O_2 caused cell death upon

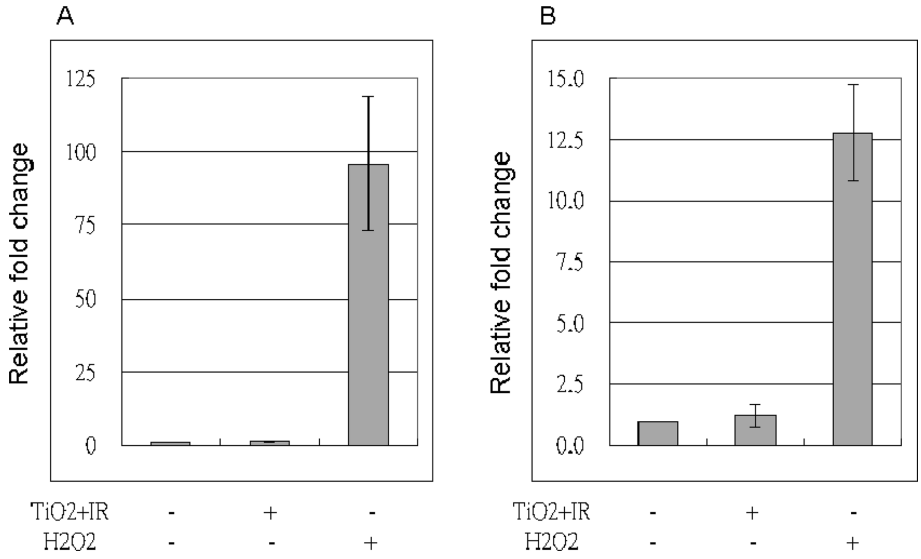

Fig. 31 Inflammation response of human A375 cells (left) and mouse embryonic fibroblasts (right) towards IR-activated TiO_2 nanofibers and H_2O_2

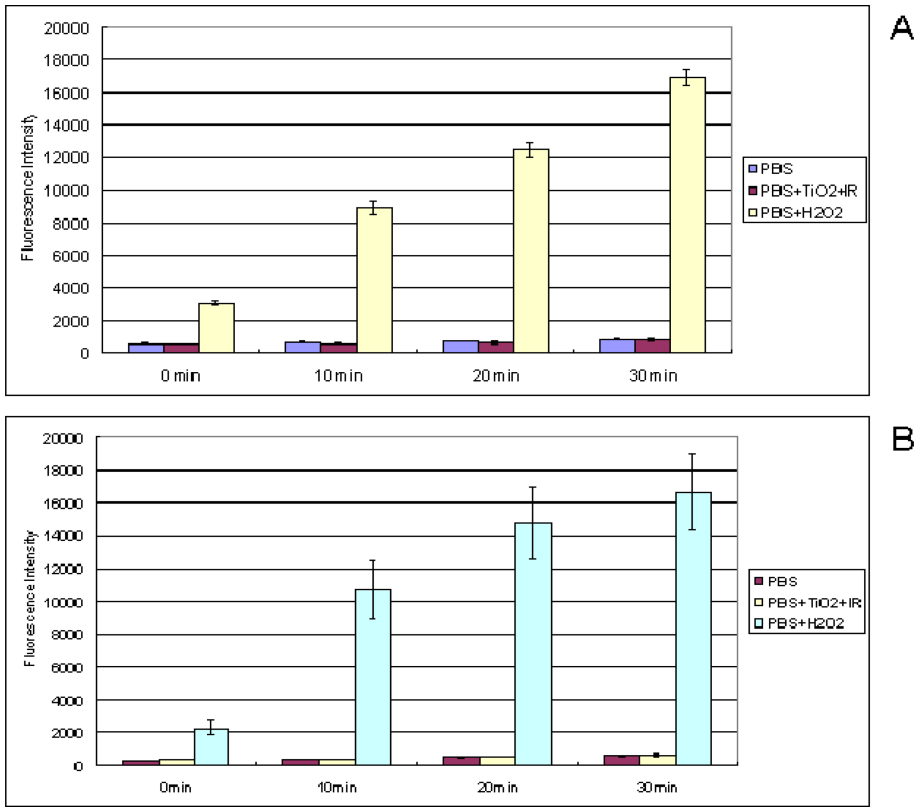

Fig. 32 Measure of up-regulation in H_2O_2 level due to IR-activated TiO_2 in human A375 cells (A) and mouse embryonic fibroblasts (B)

exposure, in both human cells and mouse fibroblasts.

As is evident from comparison with the results on untreated control group (Fig. 30), both mouse and human tissue cells showed no toxic effect when they were exposed to the titania fibers with or without IR activation, even after 6 h. On the other hand, the toxic effect of hydrogen peroxide was apparent within 3 h of exposure, as a result of depletion of the majority of the cells, quantified from the decrease in intensity of the colored stain.

The anticipated inflammatory response also was assessed in both human A375 and MEF cells in the presence of IR activated titania nanofibers and compared with that in the presence of H_2O_2 in Fig. 31. This resulted in no inflammatory response in either cell type in the presence of activated titania, while H_2O_2 induced high inflammation in both cases.

As stated earlier, increased levels of hydrogen peroxide are toxic towards human tissue cells. Hydrogen peroxide is also a byproduct of the reaction of ROS species released by TiO_2 upon activation. Therefore, H_2O_2 level in cellular tissue suspension was also monitored. This test allowed the characterization of ROS species to determine whether this toxic species is released. The results indicate that H_2O_2 levels remained unchanged in the presence of IR activated titania nanofibers immersed in phosphate buffered saline (PBS) solution with the A375 and MEF tissue cells. In comparison, H_2O_2 levels gradually increased with time, in cases where cells were treated with 0.1% H_2O_2. The variance in oxidative stresses in the A375 and MEF cells measured by fluorescence spectroscopy is illustrated in Fig. 32.

4. Conclusions

Fabrication of pure, Fe and Ag-doped TiO_2 nanofibers by electrospinning was demonstrated, using an appropriate choice of titanium and polymeric precursor, followed by calcination. This created non-woven mats of titania nanofibers with an average diameter of 150 nm. The titania nanocoatings were created on Ti and Ti6Al4V substrates by anodization and aqueous plasma electrodeposition (PED) techniques. The coatings were analyzed for their morphology and to verify their composition. In the case of anodization, nanotubular structures were produced, while PED process created fibrous and platelet morphologies on plates, and 3-dimensional extrusions in mesh and rods.

The bactericidal efficacy of nanostructured titania was evaluated in suspensions of *Staphylococcus aureus*, using confocal microscopy and a live/dead fluorescence assay by real-time imaging of the bacterial cell necrosis. In addition, the antibacterial potency of TiO_2-coated Ti mesh and Ti6Al4V rods was also evaluated. In both cases, samples were either pre- or simultaneously activated by an IR laser for 30 s to induce bactericidal effect. Both the coating methods showed excellent bacterial necrosis with the pure fibers approaching 98% necrosis of the *S. aureus* cells. In the case of doped fibers the necrosis rate was approximately 91%. 91% bacterial necrosis was also observed with pre-activated mesh and plate samples within 30 minutes after activation. In comparison, the simultaneously activated Ti6Al4V rods and anodized Ti mesh samples demonstrated 100% bacterial death.

The toxicity test showed non-life threatening effect of photoactive titania towards human and mouse tissue cells. There was also no inflammatory response or any increased level of hydrogen peroxide; all this is indicative of negative toxicity toward tissue cells. These preliminary studies assured no possible harm by the nanostructured titania toward human tissues, making them viable for application towards infection mitigation, especially in the case of surgical site infections.

References

Abramson, M.A. and Sexton, D.J. (1999), "Nosocomial methicillin-resistant and methicillin susceptible *Staphylococcus aureus* primary bacteria: at what costs?", *Infect. Cont. Hosp. Ep.*, **20**(6), 408-411.

Azad, A.-M., Dolan, S. and Akbar, S.A. (2008), "Development of agile titania sensors via high-temperature reductive etching process (HiTREP©): 1. Structural reorganization", *Int. J. Appl. Ceram. Tec.*, **5**(5), 480-489.

Azad, A.-M., Hershey, R., Aboelzahab, A. and Goel, V. (2011), "Infection mitigation efficacy of photoactive titania on orthopedic implant materials", *Adv. Orthopedics*, **2011**(ID 571652), 1-13.

Azad, A.-M., Hershey, R., Ali, S. and Goel, V. (2010), "Bactericidal efficacy of electrospun pure and Fe-doped titania nanofibers", *J. Mater. Res.*, **25**(9), 1761-1770.

Azad, A.-M., McKelvey, S. and Al-Firdaus, Z. (2008), "Fabrication of antimicrobial titania nanofibers by electrospinning", *Adv. Mater. Manuf. Testing Inform. Center Quart.*, **3**(3), 2-7.

Beiner, J.M., Grauer, J., Kwon, B.K. and Vaccaro, A.R. (2003), "Postoperative wound infections of the spine", *Neurosurg. Focus*, **15**(3), 1-5.

Bohsali, K.I., Wirth, M.A. and Rockwood, C.A. (2006), "Complications of total shoulder arthroplasty", *J. Bone Joint Surg. Br.*, **88**(10), 2279-2292.

Boland, E.D., Pawlowski, K.J., Barnes, C.P., Simpson, D.G., Wnek, G.E. and Bowlin, G.L. (2006), "Electrospinning of bioresorbable polymers for tissue engineering scaffolds", *Polym. Nanofibers: ACS Symp. Ser.*, **918**, 188-204.

Bornat, A. (1982), "Electrostatic spinning of tubular products", U.S. Patent No. 4,323,525.

Calderone, R.R., Garland, D.E., Capen, D.A. and Oster, H. (1996), "Cost of medical care for postoperative spinal infections," *Orthop. Clin. N. Am.,* **27**(1), 171-182.

Carmeli, Y., Troillet, N., Karchmer, A.W. and Samore, M.H. (1999), "Health economic outcomes of antibiotic resistance in *Pseudomonas aeruginosa*", *Arch. Intern. Med.*, **159**(10), 1127-1132.

Center for Disease Control and Prevention (2012), "Surgical Site Infection (SSI) Event", http://www.cdc.gov/nhsn/PDFs/pscManual/9pscSSIcurrent.pdf.

Chaix, C., Durand-Zaleski, I., Alberti, C. and Brun-Buisson, C. (1999), "Control of endemic methicillin-resistant *Staphylococcus aureus*: a cost-benefit analysis in an intensive care unit", *JAMA*, **282**(18), 1745-1751.

Chambers, H.F. (2001), "The changing epidemiology of *staphylococcus aureus*", *Emerg. Infect. Dis.*, **7**(2), 178-182.

Chen, G.Q. and Wu, Q. (2005), "The application of polyhydroxyalkanoates as tissue engineering materials", *Biomaterials*, **26**(33), 6565-6578.

Cluff, L.E., Reynolds, R.C., Page, D.L. and Breckenridge, J.L. (1968), "Staphylococcal bacteremia and altered host resistance", *Ann. Intern. Med.*, **69**(5), 859-873.

Cosgrove, S., Qi, Y., Kaye, K., Harbarth, S., Karchmer, A. and Carmeli, Y. (2005), "The impact of methicillin resistance in *Staphylococcus aureus* bacteremia on patient outcomes: mortality, length of stay, and hospital charges", *Infect. Cont. Hosp. Ep.*, **26**(2), 166-174.

Cosgrove, S.E., Kaye, K.S., Eliopoulos, G.M. and Carmeli, Y. (2002), "Health and economic outcomes of the emergence of third-generation cephalosporin resistance in *Enterobacter* species", *Arch. Intern. Med.*, **162**(2), 185-190.

Darouiche, R.O. (2001), "Device-associated infections: A macroproblem that starts with microadherence", *Clin. Infect. Dis.*, **33**(9), 1567-1572.

Darouiche, R.O. (2004), "Treatment of infections associated with surgical implants", *N. Engl. J. Med.*, **350**, 1422-1429.

Deresinski, S. (2005), "Methicillin-resistant *staphylococcus aureus*: An evolutionary, epidemiologic, and therapeutic odyssey", *Clin. Infect. Dis.*, **40**(4), 562-573.

Destaillats, H. (2012), "Indoor air cleaning with photocatalytic oxidation technologies", http://www.public.asu.edu/~hdestail/ research.htm

Emami-Karvani, Z. and Chehrazi, P. (2011), "Antibacterial activity of ZnO nanoparticle on gram-positive and gram-negative bacteria", *Afr. J. Microb. Res.*, **5**(12), 1368-1373.

Engemann, J.J., Carmeli, Y., Cosgrove, S.E., Fowler, V.G., Bronstein, M.Z., Trivette, S.L., Briggs, J.P., Sexton, D.J. and Kaye, K.S. (2003), "Adverse clinical and economic outcomes attributable to methicillin resistance

among patients with *staphylococcus aureus* surgical site infections", *Clin. Infect. Dis.*, **36**(5), 592-598.
Enwemeka, C.S. (2000), "Attenuation and penetration of visible 632.8 nm and invisible infra-red 904 nm light in soft tissues", *J. World Assoc. Laser Therapy*, **13**(1), 95-101.
Glassman, S.D., Dimar, J.R., Puno, R.M. and Johnson, J.R. (1996), "Salvage of instrumental lumbar fusions complicated by surgical wound infection", *Spine*, **21**(18), 2163-2169.
Griffiths, H.J. (1995), "Orthopedic complications", *Radiol. Clin. N. Am*., **33**(2), 401-410.
Hershey, R.A. (2010), *Development of titanianofibers and films for the mitigation of wound infection*, M.S. Thesis, The University of Toledo, Toledo, Ohio, U.S.A.
Holmberg, S.D., Solomon, S.L. and Blake, P.A. (1987), "Health and economic impacts of antimicrobial resistance", *Rev. Infect. Dis.*, **9**(6), 1065-1078.
How, T.V. (1985), "Synthetic vascular grafts and methods of manufacturing such grafts", U.S. Patent No. 4,552,707 .
Howden, B., Ward, P., Charles, P., Korman, T., Fuller, A., du Cros, P., Grabsch, E., Roberts, S., Robson, J., Read, K., Bak, N., Hurley, J., Johnson, P., Morris, A., Mayall, B. and Grayson, M. (2004), "Treatment outcomes for serious infections caused by Methicillin-Resistant Staphylococcus aureus with reduced vancomycin susceptibility", *Clin. Infect. Dis.*, **38**(4), 521-528.
Hwang, S., Song, J., Jung, Y., Kweon, O., Song, H. and Jang, J. (2011), "ElectrospunZnO/TiO_2 composite nanofibers as a bactericidal agent", *Chem. Commun.*, **2011**(47), 9164-9166.
Jarvis, W.R. (1996), "Selected aspects of the socioeconomic impact of nosocomial infections: morbidity, mortality, cost, and prevention", *Infect. Cont. Hosp. Ep*., **17**(8), 552-557.
Jones, T., Yeaman, M., Sakoulas, G., Yang, S.J., Proctor, R., Sahl, H.G., Schrenzel, J., Xiong, Y. and Bayer, A. (2008), "Failures in clinical treatment of *Staphylococcus aureus* infection with daptomycin are associated with alterations in surface charge, membrane phospholipid asymmetry, and drug binding", *Antimicrob. Agents Ch.*, **52**(1), 269-278.
Julander, I. (1985), "Unfavorable prognostic factors in *Staphylococcus aureus* septicemia and endocarditis", *Scand. J. Infect. Dis.*, **17**(2), 179-187.
Keidel, E. (1929), *Farben-zeitung*, **34**, 1242.
Kim, T., Oh, P.I. and Simor, A.E. (2001), "The economic impact of methicillin-resistant *Staphylococcus aureus* in Canadian hospitals", *Infect. Cont. Hosp. Ep.*, **22**(2), 99-104.
Klevens, R.M., Edwards, J.R., Richards, C.L., Horan, T.C., Gaynes, R.P., Pollock, D.A. and Cardo, D.M. (2007), "Estimating health care-associated infections and deaths in U.S. hospitals, 2002", *Public Health Rep.*, **122**(2), 160-166.
Koseki, H., Shiraishi, K., Tsurumoto, T., Asahara, T., Baba, K., Taoda, H., Terasaki, N. and Shindo, H. (2009), "Bactericidal performance of photocatalytic titanium dioxide particle mixture under ultraviolet and fluorescent light: An in vitro study", *Surf. Interface Anal.*, **41**(10), 771-774.
Levi, A.D., Dickman, C.A. and Sonntag, V.K. (1997), "Management of postoperative infections after spinal instrumentation", *J. Neurosurg.*, **86**(6), 975-980.
Lin, B., Aboelzahab, A., Azad, A.-M., Goel, V., Leaman, D., Biyani, A., Ebraheim, N. and Serhan, H. (2011), "Infrared radiation activated-nanostructured titania did not induce inflammatory responses in human cells", *Annual Meeting of the International Society for the Study of the Lumbar Spine*, Gothenburg, Sweden.
Mao, Y. and Wong, S.S. (2006), "Size- and shape-dependent transformation of nanosized titanate into analogous anatase titania nanostructures", *J. Am. Chem. Soc.*, **128**(25), 8217-8226.
Massie, J.B., Heller, J.G., Abitbol, J.J., McPherson, D. and Garfin, S.R. (1992), "Postoperative posterior spinal wound infections", *Clin. Orthop. Relat. R.*, **284**, 99-108.
Meehan, A.M., Osmon, D.R., Duffy, M.C., Hanssen, A.D. and Keating, M.R. (2003), "Outcome of penicillin-susceptible streptococcal prosthetic joint infection treated with debridement and retention of the prosthesis", *Clin. Infect. Dis.,* **36**(7), 845-849.
Minino, A.M., Arias, E., Kochanek, K.D., Murphy, S.L. and Smith, B.L. (2002), "Deaths: final data for 2000", *Nati. Vital Stat. Rep.*, **50**(15), 1-120.
Mohapatra, S.K., Mirsa, M., Mahajan, V.K. and Raja, K.S. (2007), "A novel method for the synthesis of titania nanotubes using sonoelectrochemical method and its application photoelectrochemical splitting of water", *J. Catal.*, **246**(2), 362-369.

Murray, C.K., Obremskey, W.T., Hsu, J.R., Andersen, R.C., Calhoun, J.H., Clasper, J.C., Whitman, T.J., Curry, T.K., Fleming, M.E., Wenke, J.C. and Ficke, J.R. (2011), "Prevention of infections associated with combat-related extremity injuries", *J. Trauma.*, **71**(2), 235-257.

National Nosochomial Infections Surveillance (NNIS) (2001), "System report, data summary from January 1992-June 2001", *Am. J. Infect. Control*, **29**(6), 404-421.

National Nosocomial Infections Surveillance (NNIS) (1999), "System report, data summary from January 1990-May 1999", *Am. J. Infect. Control*, **27**(6), 520.

Nichols, R.L. and Florman, S. (2001), "Clinical presentations of soft-tissue infections and surgical site infections," *Clin. Infect. Dis.*, **33**(2), 84-93.

Oka, Y., Kim, W.C., Yoshida, T., Hirashima, T., Mouri, H., Urade, H., Itoh, Y. and Kubo, T. (2008), "Efficacy of titanium dioxide photocatalyst for inhibition of bacterial colonization on percutaneous implants", *J. Biomed. Mater. Res. B*, **86B**(2), 530-540.

Olsen, M.A., Mayfield, J., Lauryssen, C., Polish, L.B., Jones, M., Vest, J. and Fraser, V.J. (2003), "Risk factors for surgical site infection in spinal surgery," *J. Neurosurg.-Spine*, **98**(2), 149-155.

Perencevich, E.N., Sands, K.E., Cosgrove, S.E., Guadagnoli, E., Meara, E. and Platt, R. (2003), "Health and economic impact of surgical site infections diagnosed after hospital discharge", *Emerg. Infect. Dis.*, **9**(2), 196-203.

Rechtine, G.R., Bono, P.L., Cahill, D., Bolesta, M.J. and Chrin, A.M. (2001), "Postoperative wound infection after instrumentation of thoracic and lumbar fractures", *J. Orthop. Trauma*, **15**(8), 566-569.

Salgado, C.D., O'Grady, N. and Farr, B.M. (2005), "Prevention and control of antimicrobial-resistant infections in intensive care patients", *Crit. Care Med.*, **33**(10), 2373-2382.

Sands, K., Vineyard, G. and Platt, R. (1196), "Surgical site infections occurring after hospital discharge", *J. Infect. Dis.*, **173**(4), 963-970.

Sarra-Bournet, C., Charles, C. and Boswell, R. (2011), "Low temperature growth of nanocrystalline TiO_2 films with Ar/O_2 low-field helicon plasma", *Surf. Coat. Tech.*, **205**(15), 3939-3946.

Sasso, R.C. and Garrido, B.J. (2008), "Postoperative spinal wound infections", *J. Am. Acad. Orthop. Sur.*, **16**(6), 330-337.

Shi, G., Cai, Q., Wang, C., Lu, N., Wang, S. and Bei, J. (2002), "Fabrication and biocompatibility of cell scaffolds of poly(L-lactic acid) and poly (L-lactic-co-glycolic acid)", *Polym. Advan. Technol.*, **13**(3-4), 227-232.

Siberry, G., Tekle, T., Carroll, K. and Dick, J. (2003), "Failure of clindamycin treatment of methicillin-resistant Staphylococcus aureus expressing inducible clindamycin resistance in vitro", *Clin. Infect. Dis.*, **37**(9), 1257-1260.

Sieradzki, K., Roberts, R., Haber, S. and Tomasz, A. (2010), "The development of vancomycin resistance in patient with methicillin-resistant Staphylococcus aureus infection", *New Engl. J. Med.*, **340**(7), 517-523.

Sill, T.J. and von Recum, H.A. (2008), "Electrospinning: applications in drug delivery and tissue engineering", *Biomaterials*, **29**(13), 1989-2006.

Simons, H.L. (1996), "Process and apparatus for producing patterned non-woven fabrics", U.S. Patent No. 3,280,229.

Smith, E.T. and Emmerson, A.M. (2000), "Surgical site infection surveillance", *J. Hosp. Infect.*, **45**(3), 173.

Stall, A.C., Becker, E., Ludwig, S.C., Gelb, D. and Poelstra, K.A. (2009), "Reduction of postoperativespinal implant infection using gentamicin microspheres", *Spine*, **34**(5), 479-483.

Styers, D., Sheehan, D.J., Hogan, P. and Sahm, D.F. (2006), "Laboratory-based surveillance of current antimicrobial resistance patterns and trends among*staphylococcus aureus*: 2005 status in the united states", *Ann. Clin. Mircrobiol. Antimicrob.*, **5**(2), 1-9.

Suwantong, O., Ruktanonchai, U. and Supaphol, P. (2010), "In vitro biological evaluation of electrospun cellulose acetate fiber mats containing asiaticoside or curcumin", *J. Biomed. Mater. Res.*, **94A**(4), 1216-1225.

Thalgott, J.S., Cotler, H.B., Sasso, R.C., LaRocca, H. and Gardner, V. (1991), "Postoperative infections in spinal implants. Classification and analysis--a multicenter study", *Spine*, **16**(8), 981-984.

Theiss, S.M., Lonstein, J.E. and Winter, R.B. (1996), "Wound infections in reconstructive spine surgery", *Orthop. Clin. N. Am.*, **27**(1), 105-110.

Whitehouse, J.D., Friedman, N.D., Kirkland, K.B., Richardson, W.J. and Sexton, D.J. (2002), "The impact of

surgical-site infections following orthopedic surgery at a community hospital and a university hospital: adverse quality of life, excess length of stay, and extra cost", *Infect. Cont. Hosp. Ep.*, **23**(4), 183-189.

Yu, J.C., Ho, W., Lin, J., Yip, H. and Wong, P.K. (2003), "Photocatalytic activity, antibacterial effect and photoinducedhydrophilicity of TiO_2 films coated on a stainless steel substrate", *Environ. Sci. Technol.*, **37**(10), 2296-2301.

Zhang, Y., Lim, C.T., Ramkrishna, S. and Huang, Z.M. (2005), "Recent development of polymer nanofibers for biomedical and biotechnological applications", *J. Mater. Sci.-Mater M.*, **16**(10), 933-946.